https://doi.org/10.31436/iiumej.v27i3.4635

A Predictive Energy Management Framework for Malaysian Residential Microgrid Using LSTM-Driven Adaptive Rule-Based Control

KAMAL AKASHAH CHE KAMARUDDIN, SITI HAJAR YUSOFF*, TEDDY SURYA GUNAWAN, SARAH YASMIN MOHAMAD, AISHA HASSAN ABDALLA HASHIM, NUR SHAHIDA MIDI

Department of Electrical and Computer Engineering, International Islamic University Malaysia, Kuala Lumpur, Malaysia

**Corresponding author: sitiyusoff@iium.edu.my*

(Received: 17 July 2026; Accepted: 19 August 2026; Published online: 11 September 2026)

ABSTRACT: The rapid increase in global energy demand and the growing emphasis on environmental sustainability have accelerated the integration of renewable energy sources (RES) into modern microgrids. However, the stochastic nature of RES, the unpredictable behavior of load demand, and the variability of utility electricity tariffs under the Time of Use (ToU) pricing mechanism increase the operational complexity of microgrid energy management systems (EMS). To address these challenges, this research focuses on developing and implementing a hybrid EMS that integrates machine learning (ML)-based Long Short-Term Memory (LSTM) predictive models with conventional Rule-based Control (RBC) strategies for tertiary-level control of a centralized, grid-connected residential microgrid. The proposed EMS approach combines one-hour-ahead forecasts of solar Photovoltaic (PV) energy generation and residential load demand with predefined Load Following (LF) and Cycle Charging (CC) control strategies, enabling the EMS to anticipate future operating conditions while preserving the simplicity of the conventional RBC framework. The main objective of this research is to evaluate whether integrating LSTM predictive models into conventional RBC strategies can reduce the total operating cost of a Malaysian residential microgrid under the applicable ToU electricity tariff and Solar Accelerated Transition Action Program (Solar ATAP) scheme. The microgrid is modeled in MATLAB Simulink as a grid-connected system comprising a solar PV system, battery energy storage system (BESS), and three residential load profiles representing terrace, apartment, and condominium households in Kuala Lumpur, Malaysia. The data used to develop the proposed hybrid EMS are sourced from various trusted platforms, including Tenaga Nasional Berhad (TNB) energy smart meters, Huawei FusionSolar, and Solcast. The simulation results showed that the developed LSTM predictive models achieved higher forecasting accuracy for both solar PV energy generation and residential load demand than the baseline Feedforward Neural Network (FFNN) models. Leveraging these forecasts, the proposed LSTM-RBC-based EMS effectively coordinated the distributed energy resources (DERs) under the ToU electricity tariff and Solar ATAP scheme by strategically scheduling BESS charging and discharging operations and managing grid energy import and export based on economic operating conditions. The proposed hybrid EMS achieved a significant reduction in total operating cost by approximately 30% to 40% compared with conventional RBC strategies under different initial BESS State of Charge (SoC) scenarios. These results demonstrate that integrating ML-based LSTM predictive models into conventional RBC strategies enables more economical microgrid operation, highlighting the potential of predictive control to improve the operational performance of residential microgrids.

ABSTRAK: Peningkatan pesat dalam permintaan tenaga global serta penekanan yang semakin meningkat terhadap kelestarian alam sekitar telah mempercepat integrasi sumber tenaga boleh baharu (RES) ke dalam mikrogrid moden. Walau bagaimanapun, sifat stokastik RES, ketidakpastian tingkah laku permintaan beban, serta perubahan tarif elektrik utiliti di bawah mekanisme harga Masa Penggunaan (ToU) telah meningkatkan kerumitan operasi sistem pengurusan tenaga (EMS) mikrogrid. Bagi menangani cabaran ini, kajian ini memberi tumpuan kepada pembangunan dan pelaksanaan EMS hibrid yang mengintegrasi model ramalan Ingatan Jangka Pendek Berpanjangan (LSTM) berasaskan pembelajaran mesin (ML) dengan strategi konvensional Kawalan Berasaskan Peraturan (RBC) bagi kawalan peringkat tertier untuk mikrogrid kediaman berpusat yang disambungkan kepada grid. Pendekatan EMS ini menggabungkan ramalan satu jam ke hadapan bagi penjanaan tenaga solar foto volta (PV) dan permintaan beban kediaman dengan strategi kawalan Pengikutan Beban (LF) dan Kitar Pengecasan (CC) yang telah ditetapkan, bagi membolehkan EMS menjangka keadaan operasi pada masa hadapan sambil mengekalkan kesederhanaan kerangka RBC konvensional. Objektif utama kajian ini adalah bagi menilai sama ada integrasi model ramalan LSTM ke dalam strategi RBC konvensional dapat mengurangkan jumlah kos operasi mikrogrid kediaman di Malaysia di bawah tarif elektrik ToU yang berkuat kuasa dan skim Program Solar Accelerated Transition Action Programme (Solar ATAP). Mikrogrid tersebut dimodelkan dalam MATLAB Simulink sebagai sistem yang disambung kepada grid dan terdiri daripada sistem solar PV, sistem penyimpanan tenaga bateri (BESS), serta tiga profil beban kediaman yang mewakili rumah teres, apartmen, dan kondominium di Kuala Lumpur, Malaysia. Data yang digunakan dalam pembangunan EMS hibrid ini diperoleh dari beberapa platform yang dipercayai, termasuk meter pintar tenaga Tenaga Nasional Berhad (TNB), Huawei FusionSolar, dan Solcast. Hasil simulasi menunjukkan bahawa model ramalan LSTM yang dibangunkan mencapai ketepatan ramalan lebih tinggi bagi kedua-dua penjanaan tenaga solar PV dan permintaan beban kediaman berbanding model asas Rangkaian Neural Suap ke Depan (FFNN). Melalui ramalan ini, EMS berasaskan LSTM-RBC berjaya menyelaras sumber tenaga teragih (DERs) dengan berkesan di bawah tarif elektrik ToU dan skim Program Solar ATAP melalui penjadualan strategik operasi pengecasan dan nyahcas BESS, serta pengurusan import dan eksport tenaga grid berdasarkan keadaan operasi yang lebih ekonomik. EMS hibrid ini mencapai pengurangan ketara dalam jumlah kos operasi, iaitu kira-kira 30% hingga 40% berbanding strategi RBC konvensional di bawah senario keadaan cas awal (SoC) BESS berbeza. Dapatan ini menunjukkan bahawa pengintegrasian model ramalan LSTM berasaskan ML ke dalam strategi RBC konvensional membolehkan operasi mikrogrid yang lebih ekonomik, sekaligus menonjolkan potensi kawalan ramalan dalam meningkatkan prestasi operasi mikrogrid kediaman.

KEYWORDS: *Energy Management Systems (EMS), Long Short-Term Memory (LSTM), Machine Learning (ML), Rule-Based Control (RBC), Tertiary-Level Control*

1. INTRODUCTION

A microgrid, as the term suggests, is a localized or autonomous electrical network that can produce, consume, store, and control energy flow within its boundaries. It typically involves multiple distributed energy resources (DERs), including both dispatchable and non-dispatchable units such as solar Photovoltaic (PV), wind turbines, battery energy storage systems (BESS), diesel generators (DG), and fuel cells. Integrating these energy resources improves the microgrid's flexibility to adapt quickly to changes in generation, storage, and demand, while also increasing reliability in maintaining power supply during grid outages. However, high penetration of renewable energy sources (RES) in modern microgrids introduces significant operational challenges, primarily because of their inherent stochastic and intermittent nature. RES depend heavily on weather conditions, which can result in inconsistent power generation and system instability. For instance, solar PV systems rely heavily on sunlight availability, and wind turbine output fluctuates with varying wind speed.

Microgrids are dynamic in nature since they have the capability of operating in multiple modes, including islanded, grid-connected, or shut down [1]. Microgrids can seamlessly connect and disconnect from the main grid at any time. In islanded mode, the microgrid supplies power to the local consumers without being connected to the main grid, whereas in grid-connected mode, it operates in synchronization with the main grid, enabling power exchange and enhanced reliability. Shut-down mode is normally used for maintenance, fault conditions, or system protection purposes. Microgrids can operate across a wide range of voltage levels, from low-voltage systems (230V single-phase and 400V three-phase) to medium voltage levels such as 11kV and 33kV. In Malaysia, microgrids operate using the same regulated voltage standards applied to the national distribution network to ensure compliance with the Malaysian Grid Code, Distribution Code, and MS IEC60038 voltage standard [2].

Solar PV systems are currently the fastest-growing RES in Malaysia, with a growth rate expectation of 13.46% by 2035 [3]. The rapid expansion of solar PV is due to the country's strategic equatorial location and consistent year-round climate, which provide abundant solar irradiance. Moreover, government-led initiatives such as the Feed-in Tariff (FiT), Net Energy Metering (NEM), and the Solar Accelerated Transition Action Program (Solar ATAP) have further encouraged consumers to adopt solar PV systems. However, the increasing integration of solar PV systems in Malaysia may lead to system instability due to intermittency and uncertainty of energy generation, thereby necessitating more advanced energy management systems (EMS).

In modern microgrid development, EMS is regarded as the core component, responsible for coordinating energy resources and making optimal control decisions. Optimal control decisions typically focus on minimizing operating costs, maximizing power generation, extending the lifespan of the energy storage system (ESS), and ensuring a consistent electricity supply to consumers. According to [4], the essential aspects of microgrid control that must be addressed are: load tracking, real and reactive power control, voltage regulation, frequency regulation, load sharing, and protection.

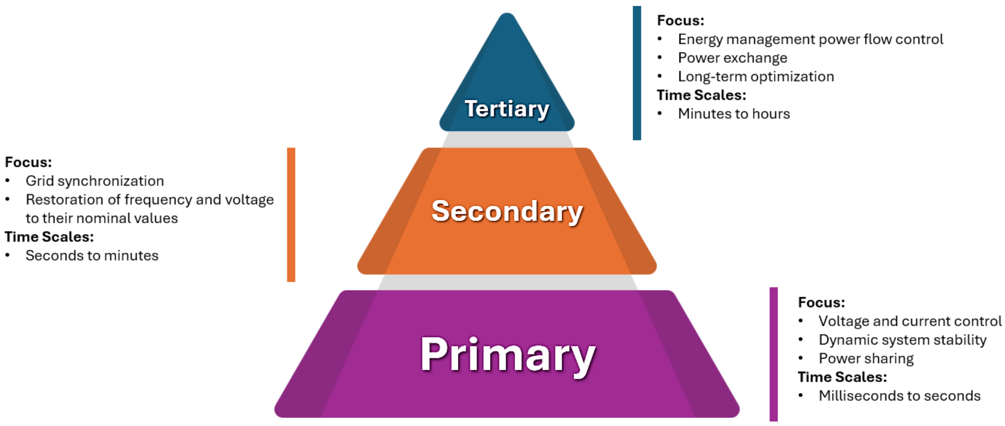

Figure 1. Hierarchical control levels of microgrids

Microgrid EMS has three hierarchical control levels: primary, secondary, and tertiary control, as shown in **Figure 1**. Each control level features different functions, objectives, and time scales [5]. Primary-level control serves as the basis of hierarchical control in microgrid EMS and is important for fast voltage and frequency stabilization, as well as effective power sharing among the DERs in the microgrid. This control layer is implemented locally at the inverter or DER level and operates on time scales of milliseconds to seconds. Secondary-level control, on the other hand, focuses on restoring voltage and frequency to their nominal values and improves grid synchronization during transitions between microgrid operation modes. This control layer operates at slower time scales, between seconds and minutes, depending on the communication infrastructure. Finally, tertiary-level control is the highest level in hierarchical microgrid control. This control layer focuses on the long-term optimization of the microgrid's EMS in terms of economic dispatch, power scheduling, system constraints, or power exchanges between microgrids and external networks. Tertiary-level control generally works on time scales ranging from several minutes to hours.

While hierarchical control levels describe the focus and time-scale separation of microgrid EMS, practical implementation can use different control structures, such as centralized, decentralized, or distributed approaches. In a centralized control structure, a single central EMS controller collects all system information from the DERs and makes operational decisions for the entire microgrid. This structure provides strong system-wide coordination and can deliver high optimization performance, as the controller has full visibility of the microgrid. It can be advantageous for microgrids with small resources and relatively low demand. However, this structure scales poorly as the system expands and is highly vulnerable to a single point of failure, where a central controller failure may disrupt the entire EMS operation. In contrast, a decentralized control structure allows each subsystem to operate with its own local controller, thereby enabling independent decision-making based on local objectives. Compared to the centralized control structure, this structure offers improved reliability and scalability. However, it often results in suboptimal performance due to the lack of global coordination. Meanwhile, the distributed control structure allows multiple controllers to communicate and cooperate to achieve common control objectives without relying entirely on a single central controller. Compared to the centralized control structure, this structure offers greater scalability, while also providing better coordination than the decentralized approach, despite being more complex to implement [6]. **Figure 2** summarizes the microgrids classification based on operational modes, control levels, control structures, and configurations.

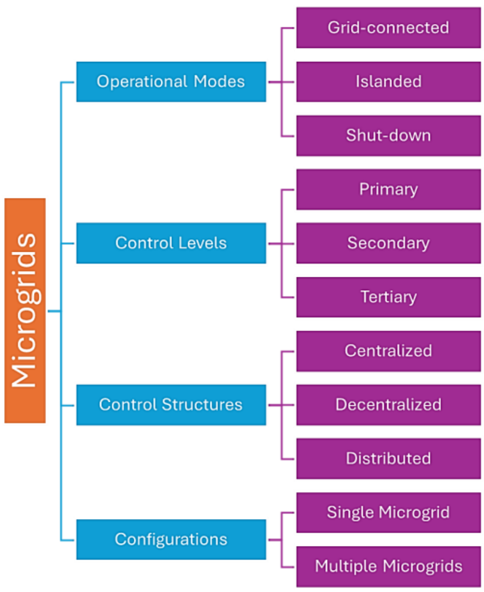

Figure 2. Microgrids classification based on operational modes, control levels, control structures, and configurations

Numerous methods have been proposed for tertiary-level microgrid EMS in the literature. Among these, heuristic Rule-based Control (RBC) is one of the most straightforward and widely adopted approaches, which operates based on predefined "if-then" rules that make it simple to design, implement, and interpret [7]. The study in [8] implemented a centralized RBC-based EMS strategy to examine the techno-economic and environmental performance of an isolated microgrid comprised of a solar PV system, DG, and BESS. The study compared and evaluated the performance of three distinct RBC control strategies known as Load Following (LF), Cycle Charging (CC), and Combined Dispatch (CD), with their performance metrics assessed based on the Net Present Cost (NPC), Cost of Energy (COE), and Carbon Dioxide (CO2) emissions. The results showed that CD achieved the lowest NPC, COE, and CO2 emissions compared to LF and CC. On the other hand, the research in [9] focused on optimizing the operational cost of a grid-connected microgrid consisting of a solar PV system and BESS using a centralized RBC-based EMS strategy. The proposed EMS considered Time of Use (ToU) electricity pricing and the maximum sanctioned limits for power imported from the grid. This research successfully optimized overall energy consumption costs and effectively managed peak demand by controlling the BESS based on real system states and ToU. The study in [10] implemented a centralized RBC-based EMS strategy for an off-grid electric vehicle (EV) charging station integrated with a solar PV system and BESS, where the EV load demand was dynamically modeled using home charging data from metropolitan Melbourne, Australia. The simulations considered three scenarios: sunny, cloudy, and nighttime conditions. The proposed EMS demonstrated stable direct-current (DC) bus operation within ±5%, the ability to operate independently of the grid, and effective BESS operation within safe State of Charge (SoC) levels of 25% to 95%. Despite the encouraging results shown in [8]-[10], the EMS based on the RBC strategy does not guarantee optimal microgrid operation, particularly under dynamic and uncertain operating conditions, because it depends on predefined control rules.

To enhance the responsiveness of EMS, some studies have implemented a Model Predictive Control (MPC) strategy, which uses mathematical models to forecast future system states and optimize operation at each timestep [11]. The work in [12] focused on developing a robust and practical centralized EMS based on the integrated MPC and RBC strategy for a grid-connected microgrid comprised of solar PV and BESS. MPC was employed as the first control layer to determine the optimal BESS SoC, aiming to keep the microgrid's operation within the white zone, where system constraints are comfortably satisfied. Meanwhile, RBC served as the second control layer to ensure operational safety and constraint satisfaction. However, this strategy resulted in a slight increase in daily operating cost compared to conventional MPC. The study in [11] further improved the centralized EMS based on MPC by integrating it with an Artificial Neural Network (ANN), which is a subset of Machine Learning (ML). ANN was used to predict solar PV energy generation, whereas MPC was used to manage peak demand and optimize energy usage through load curtailment and load shifting. This hybrid EMS approach reduced grid energy usage and associated costs by up to 48% and 34% on sunny and cloudy days, respectively.

Another study in [13] combined ANN with the metaheuristic Artificial Bee Colony algorithm into a centralized EMS to achieve optimal power flow control for a home EMS in a residential microgrid connected to the main grid, solar PV, and BESS. The proposed EMS achieved significant reductions in electricity consumption cost of 9.05% during non-summer months and 29.7% during summer months compared to the RBC-only strategy. The work in [14] also employed a metaheuristic algorithm, namely Particle Swarm Optimization (PSO), integrated with the RBC strategy into a distributed EMS to optimize energy management within community-based grid-connected residential microgrids comprising solar PV and BESS. PSO was used in the first control layer to determine optimal load scheduling, while RBC was applied in the second control layer to perform peak demand shaving by regulating the BESS charging and discharging schedule. This hybrid EMS approach achieved an average improvement of

https://doi.org/10.31436/iiumej.v27i3.4635

8.5% in Percentage Peak Shaving (PPS) across various PV power and load demand patterns for both winter and summer conditions.

To maintain the simplicity of RBC while enhancing its decision-making capability and adaptability, many studies have integrated ML techniques with the RBC strategy. The work in [15] compared the performance of four different ML techniques, known as Decision Tree, Random Forest, Deep ANN, and Long Short-Term Memory (LSTM), for forecasting RES generation and load consumption. These forecasting models were then integrated into a centralized RBC-based EMS framework for an islanded microgrid comprising solar PV, wind turbines, BESS, DG, and a fuel cell, focusing on improving scheduling performance through peak shaving and valley filling. The results indicated that the LSTM model performed best in forecasting RES generation and load demand, while the ML-based EMS demonstrated greater robustness to uncertainties in RES generation and load demand. Similar to [15], the work in [16] implemented a Temporal Convolutional Neural Network predictive model, which was subsequently integrated into a centralized RBC-based EMS framework. However, the proposed hybrid EMS considered a power flow algorithm that coordinated RES utilization and ToU pricing to improve the economic operation of the BESS. The study in [17] adopted a slightly different approach, in which the centralized EMS used a dynamic decision-making mechanism capable of switching between RBC and deep learning models. RBC served as a foundational method by providing a decision-making framework based on predefined logic and rules to manage various energy resources, demand responses, and microgrid components. Conversely, the deep learning models were only used for adaptive control actions, particularly when rules might be inadequate or under unexpected conditions.

This study proposes a hybrid approach that integrates an ML-based LSTM predictive model with conventional RBC strategies for tertiary-level control of a centralized, grid-connected residential microgrid, with specific consideration of the Malaysian operating context. The microgrid is configured as a grid-connected system consisting of a solar PV system, BESS, and three types of Malaysian residential loads, all modeled in MATLAB Simulink. The core objective of this study is to investigate whether the proposed hybrid EMS can reduce the total operating cost of the residential microgrid through more economical DER coordination under the Malaysian ToU electricity tariff and Solar ATAP scheme. The main contributions of this study are the development, implementation, and evaluation of the proposed LSTM-RBC-based EMS, with the details as follows:

- Development of ML-based LSTM predictive models for one-hour-ahead forecasting of solar PV energy generation and residential load demand.
- Development of forecast-informed adaptive RBC strategies that integrate one-hour-ahead LSTM predictions and upcoming ToU electricity tariff information into the decision-making process of the conventional LF and CC strategies.
- Implementation and evaluation of the proposed LSTM-RBC-based EMS using Malaysian residential load profiles, solar PV generation, weather data, and electricity tariff conditions to analyze its applicability and economic performance under the Malaysian ToU tariff and Solar ATAP scheme.
- Evaluation of the economic and operational trade-offs introduced by the proposed hybrid EMS in terms of total operating cost, grid energy exchange, BESS degradation cost, self-sufficiency ratio (SSR), PV utilization, and BESS SoC behavior under different initial BESS SoC conditions.

The rest of this paper is structured as follows: methodology, followed by results and discussion, and finally, the conclusion.

2. METHODOLOGY

2.1. General Framework of the Proposed Microgrid and Hybrid EMS

In this study, the proposed microgrid system operates as a grid-connected system comprising a solar PV system, BESS, and three Malaysian residential load profiles, as shown in **Figure 3**.

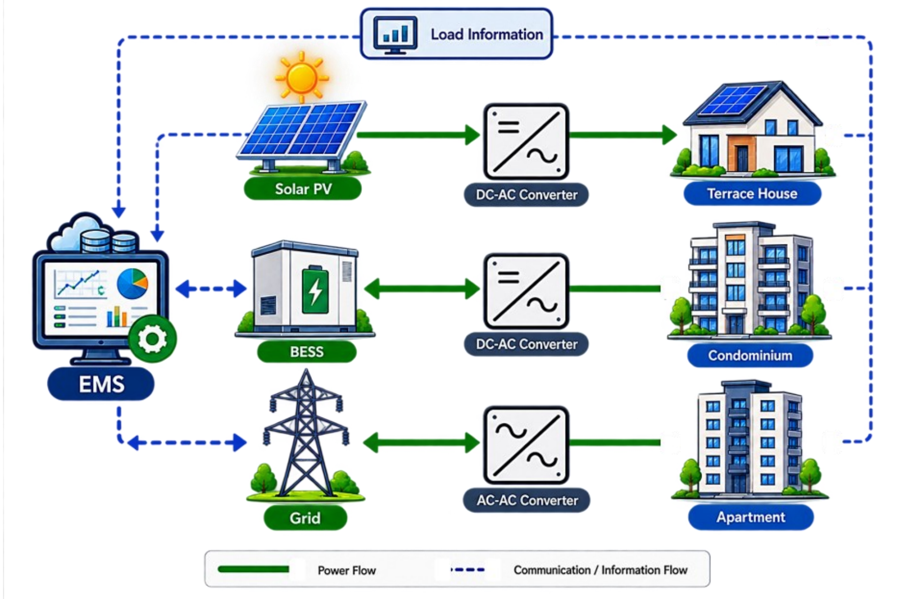

Figure 3. Proposed grid-connected microgrid system

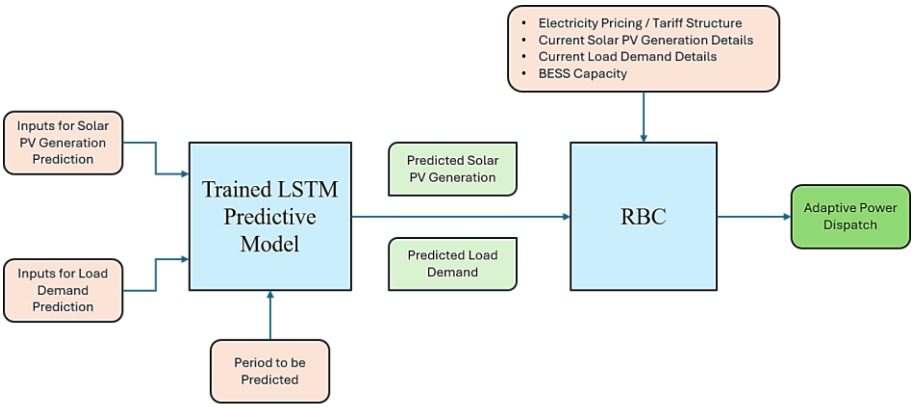

Figure 4. Proposed LSTM-RBC-based EMS framework

The proposed microgrid system prioritizes energy supply from the solar PV system, followed by the BESS, and finally the main grid. The solar PV system operates at its maximum power point to maximize solar energy generation, while the BESS stabilizes microgrid operation. For this study, the BESS is assumed to be charged only using surplus energy generated by the solar PV system, while grid charging is not considered. Moreover, the BESS is not intentionally discharged to export stored energy to the main grid and capture economic benefits from periods of higher electricity prices. These BESS operating assumptions emphasize self-consumption and the effective utilization of locally generated renewable energy. The main grid serves as a backup energy source for the microgrid only when the combined available power from the solar PV system and BESS is insufficient to meet the residential load demand. **Figure 3** also illustrates the communication flow between the centralized EMS and the solar PV system, BESS, main grid, and residential loads.

Figure 4 shows the proposed LSTM-RBC-based EMS framework in this study, featuring an LSTM predictive model and RBC in a cascaded configuration. The proposed EMS begins by forecasting solar PV energy generation and load demand using the trained LSTM predictive models. The RBC then uses these predictions, along with required local information, to provide adaptive power-dispatch decisions for the dispatchable DERs.

2.2. Data Collection

This study considers four types of data: weather data, load demand data, solar PV energy generation data, and energy price data. All datasets were sourced from reputable sources to ensure data quality, reliability, and accuracy, which are essential for developing a robust LSTM predictive model and an efficient EMS.

2.2.1. Weather Data

Weather data is an essential component of the dataset, providing valuable insights into the environmental factors that influence solar PV energy generation. This dataset was obtained from Solcast, a data service platform that provides up to 20 years of historical data. In this study, the weather dataset comprises 5415 hourly observations recorded between August 2025 and March 2026. Each observation contains five weather variables: air temperature, global horizontal irradiance (GHI), water precipitation, water precipitation rate, and relative humidity, resulting in a total of 27075 samples. The weather dataset corresponds to a specific geographical location at coordinates (3.1864, 101.7059), near Kuala Lumpur, Malaysia, as shown in **Figure 5**.

Figure 5. Location coordinates (3.1864, 101.7059) in Kuala Lumpur, Malaysia

2.2.2. Solar PV Energy Generation Data

Solar PV energy generation data was collected via the Huawei FusionSolar monitoring platform from an in-house solar PV system installed within the same geographical area, as illustrated in **Figure 5**. The solar PV system consists of nine 620 W Trina TSM-NEG19R.20-620 solar panels with a total capacity of 5.58 kWp and a 5 kWac Huawei SUN2000-5KTL-L-1 inverter, with detailed specifications provided in **Table 1**.

A total of 5415 hourly solar PV energy generation samples were obtained for the period spanning from August 2025 to March 2026, as depicted in **Figure 6**. **Figure 7** presents the average hourly solar PV energy generation, with peak sun hours typically occurring for 5 hours between 10 am and 3 pm at the selected location.

Table 1. Solar PV systems parameters

PV Panel TSM-NEG19R.20-620 @ Standard Test Condition (STC)	
Peak Power (P_{max})	620 W
Maximum Power Voltage (V_{mpp})	41.4 V
Maximum Power Current (I_{mpp})	14.99 A
Open Circuit Voltage (V_{oc})	49.6 V
Short Circuit Current (I_{sc})	15.91 A
Module Efficiency (η_{pv})	23.0 %
Inverter SUN2000-5KTL-L-1	
Maximum PV power	7500 Wp
Maximum Input Voltage	600 V
Startup Voltage	100 V
Maximum Power Point Tracking (MPPT) Operating Range	90 V – 560 V
Rated Input Voltage	360 V
Maximum Input Current per MPPT	12.5 A
Maximum I_{sc}	18 A
Inverter Efficiency (η_{inv})	98.4 %

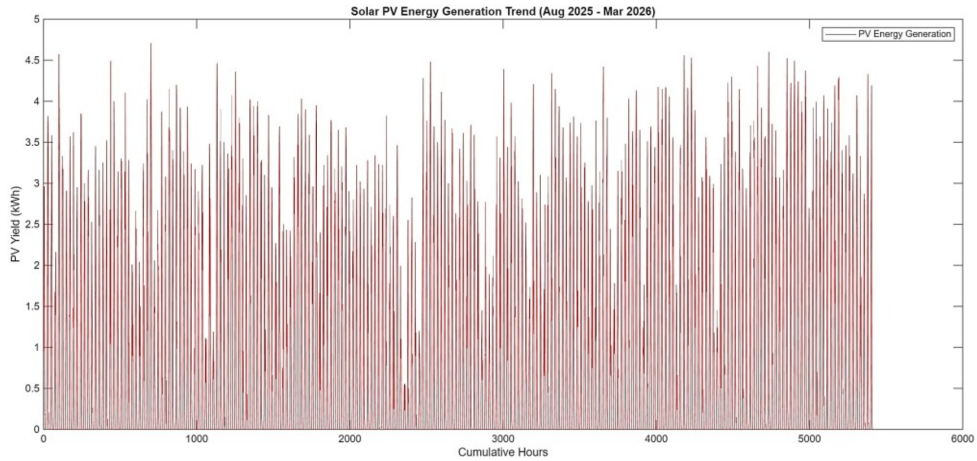

Figure 6. Solar PV energy generation trend between August 2025 and March 2026

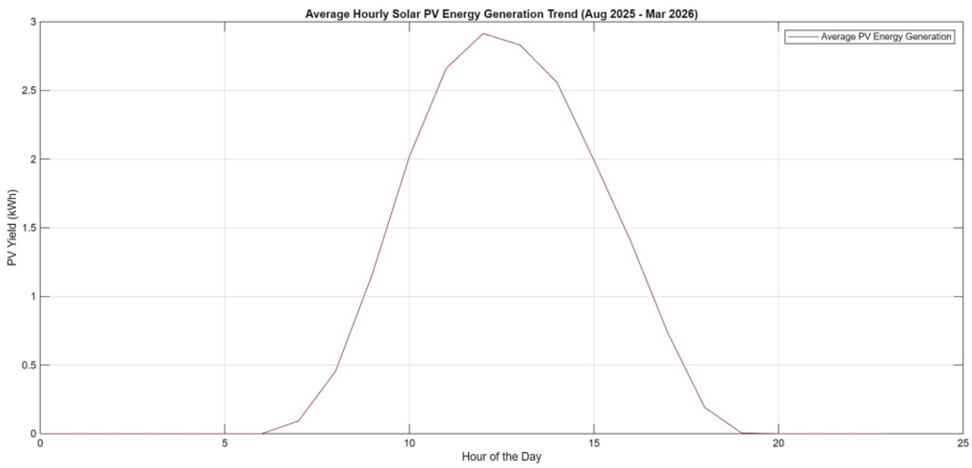

Figure 7. Average hourly solar PV energy generation trend between August 2025 and March 2026

2.2.3. Load Demand Data

This study considers three types of Malaysian residential load profiles located within the same geographical area, as shown in **Figure 5**, namely terrace house, apartment, and condominium, using the data sourced from Tenaga Nasional Berhad (TNB)'s energy smart meter platform. This platform facilitates the analysis of the historical hourly load demand patterns. A total of 32760 samples were collected, spanning from January 2025 to March 2026, comprising 10920 samples for each residential type. Considering different residential load types is important to improve the LSTM predictive model's generalization across different housing scenarios. **Figure 8** shows the Malaysian residential load demand trends, with average electricity consumption of 0.67 kWh for the terrace house, 0.43 kWh for the apartment, and 0.37 kWh for the condominium.

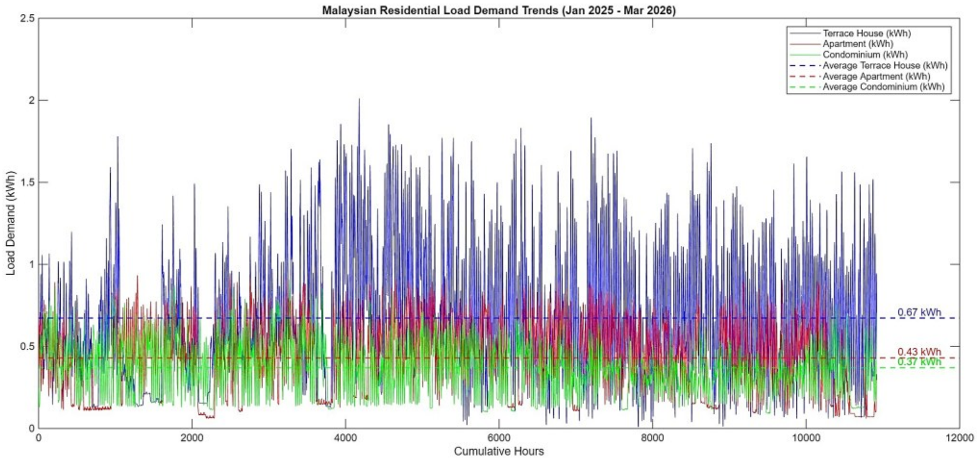

Figure 8. Malaysian residential load profiles for three different types of Malaysian residential houses between January 2025 and March 2026

2.2.4. Grid Energy Pricing based on ToU λ_{ToU}

In Malaysia, TNB introduced the ToU electricity tariff starting in July 2025 as part of the government's electricity tariff restructuring, which provides consumers with differentiated rates based on peak and off-peak hours. The peak tariff applies only on weekdays from 2 pm to 10 pm, while the off-peak tariff applies from 10 pm to 2 pm on weekdays and throughout the day on weekends and public holidays. **Table 2** shows the ToU electricity tariff applied to domestic consumers in Malaysia.

Table 2. Malaysian domestic ToU electricity tariff as of July 2025 [18]

Domestic ToU Electricity Tariff		
For total consumption of 1500 kWh and below per month		
Peak Energy Charge, C_{peak}	RM/kWh	0.2852
Off-peak Energy Charge, $C_{offpeak}$	RM/kWh	0.2443
Capacity Charge, $C_{capacity}$	RM/kWh	0.0455
Network Charge, $C_{network}$	RM/kWh	0.1285
Retail Charge, C_{retail}	RM/month	10.00
For total consumption of more than 1500 kWh per month		
Peak Energy Charge, C_{peak}	RM/kWh	0.3852
Off-peak Energy Charge, $C_{offpeak}$	RM/kWh	0.3443
Capacity Charge, $C_{capacity}$	RM/kWh	0.0455
Network Charge, $C_{network}$	RM/kWh	0.1285
Retail Charge, C_{retail}	RM/month	10.00

https://doi.org/10.31436/iiumej.v27i3.4635

2.2.5. Solar ATAP Export Energy Offset Rate λ_{ATAP}

Solar ATAP is a rooftop solar scheme introduced by the Malaysian government in January 2026 to further accelerate the adoption of solar PV systems. The scheme serves as a successor to the NEM while preserving its core principles. Under the NEM scheme, excess energy generated by the solar PV system is credited on a one-to-one energy-offset basis, whereas Solar ATAP implements an energy-offset mechanism based on the applicable electricity tariff. According to [19], the energy exported to the main grid under Solar ATAP is offset against the bill at a rate ranging from RM 0.27 to RM 0.37 per kWh for the residential consumers. In this study, the export energy offset rate is assumed to be RM 0.37 per kWh.

2.3. Data Preprocessing

All previously collected datasets were preprocessed in MATLAB before developing LSTM predictive models. The data preprocessing procedures consisted of feature selection, data cleaning, chronological data splitting, and data normalization. Feature selection was performed first to identify the input variables that significantly influence the LSTM models' forecasting performance. For the solar PV energy generation prediction model, the selected input features include:

- Hour of the day
- Month of the year
- Air temperature
- GHI
- Water precipitation
- Water precipitation rate
- Relative humidity
- Current PV yield
- PV yield recorded at 1-hour intervals over the previous 24 hours

For the residential load demand prediction model, the selected input features comprise:

- Hour of the day
- Month of the year
- Day of the week
- Type of day
- Type of house
- Current load demand
- Load demand recorded at 1-hour intervals over the previous 24 hours

Subsequently, the datasets were cleaned using the MATLAB Data cleaner, which involved outlier detection and removal through Z-score filtering, followed by outlier replacement and missing-value handling using linear interpolation, and finally a causal data-smoothing procedure to reduce measurement noise. Next, the datasets were arranged chronologically and split into training, validation, and testing subsets using a 70:20:10 ratio. This chronological splitting strategy ensured that the training, validation, and testing datasets followed the natural temporal sequence of the data, thereby preventing temporal data leakage from future observations into the model training process. Finally, the data normalization process was performed using the min-max technique, as expressed in Eq. (1), to ensure consistent input conditions for the LSTM predictive model.

$$x_{norm} = \frac{x - x_{min}}{x_{max} - x_{min}} \tag{1}$$

https://doi.org/10.31436/iiumej.v27i3.4635

where x_{norm} is the normalized data, x is the data value, x_{min} is the minimum data value, and x_{max} is the maximum data value.

2.4. LSTM Predictive Modeling

Among the various ANN-based predictive models, the LSTM predictive model has been selected for forecasting solar PV energy generation and load demand due to its effectiveness in capturing both short- and long-term temporal dependencies, as demonstrated in the previous study [15]. LSTM, a variant of Recurrent Neural Network (RNN), can model sequential data while mitigating the vanishing and exploding gradient problems that commonly occur in conventional RNNs. **Figure 9** shows the structure of a single LSTM cell that is controlled by three main gates known as the Forget gate, Input gate, and Output gate. These gates will determine whether the information should be retained, updated, or discarded.

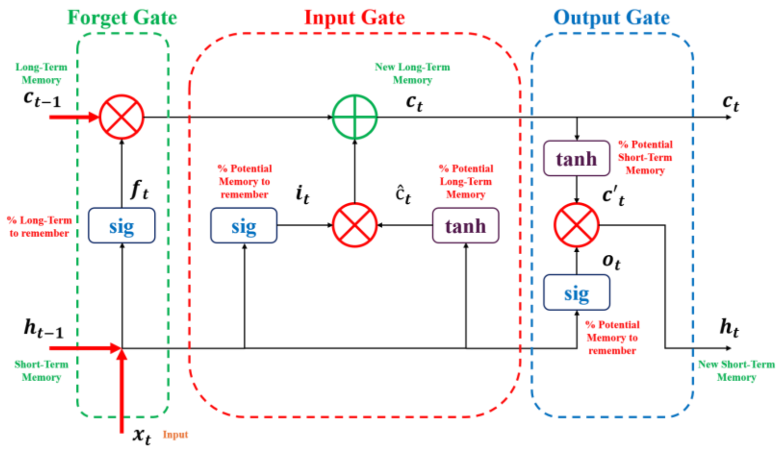

Figure 9. Structure of a single LSTM cell

According to **Figure 9**, the forget gate contains a sigmoid activation function that determines the percentage of long-term memory from the previous cell state to be remembered. This percentage can be calculated using Eq. (2).

$$f_t = \sigma\left(W_f \cdot [h_{t-1}, x_t] + b_f\right) \tag{2}$$

where σ is a sigmoid function, W_f is the weight matrix associated with the forget gate, h_{t-1} is the previous hidden state, x_t is the current input, and b_f is the forget gate bias.

Next, the input gate consists of two activation functions, sigmoid and hyperbolic tangent, used to determine the percentage of new information to be remembered and to create candidate values representing potential updates to memory, respectively. The new memory percentage can be calculated using Eq. (3), whereas the memory potential update percentage is determined according to Eq. (4). The current cell state, c_t, can be calculated as in Eq. (5) by adding the new candidate values calculated from the multiplication of i_t and $\hat{c}_t$, with the multiplication of the previous state c_{t-1} with f_t.

$$i_t = \sigma\left(W_i \cdot [h_{t-1}, x_t] + b_i\right) \tag{3}$$

$$\hat{c}_t = tanh(W_c \cdot [h_{t-1}, x_t] + b_c) \tag{4}$$

$$c_t = f_t \cdot c_{t-1} + i_t \cdot \hat{c}_t \tag{5}$$

where $tanh$ is a hyperbolic tangent function, W_i and W_c are the weight matrices associated with the input gate for the sigmoid and hyperbolic tangent functions, respectively, and b_i and

https://doi.org/10.31436/iiumej.v27i3.4635

b_c are the biases of the input gate for the sigmoid and hyperbolic tangent functions, respectively.

Finally, the output gate contains two activation functions: the sigmoid and hyperbolic tangent functions. The sigmoid function is used to determine the percentage of potential memory to be the output, whereas the hyperbolic tangent function is used to scale the cell state value c_t to a normalized range between -1 and 1 before it is filtered by the sigmoid function of the output gate. The calculation of the potential memory percentage to be the output is as in Eq. (6), while the scaling of the cell state value can be done using Eq. (7). By multiplying Eq. (6) and Eq. (7), the hidden state, h_t, can be calculated as in Eq. (8).

$$o_t = \sigma(W_o \cdot [h_{t-1}, x_t] + b_o) \tag{6}$$

$$c'_t = tanh(c_t) \tag{7}$$

$$h_t = o_t \cdot c'_t \tag{8}$$

where W_o and b_o are the weight matrix and bias associated with the output gate, respectively.

2.4.1. LSTM Training Settings and Performance Metrics

In this research, the LSTM predictive model for solar PV energy generation consisted of a single input layer of 32 neurons (corresponding to the 32 selected input features), a single hidden layer of 50 neurons, and a single output neuron. Similarly, for load demand prediction, the LSTM had a single input layer of 30 neurons (corresponding to the 30 selected input features), a single hidden layer of 50 neurons, and a single output neuron. For both predictive models, a hidden layer with 50 neurons was selected to provide adequate prediction capability while maintaining a simple model structure. The final output layer in both predictive models represents the predicted value for the next time step (one-hour ahead). This short-term prediction horizon is implemented to balance forecasting accuracy and model complexity, as prediction performance typically declines for longer horizons [20]. The number of training epochs was set to 2000 based on the observation that training and validation losses approached convergence within this range. Both models were optimized using the Adam optimizer with a constant learning rate of 0.01. This learning rate was selected based on the observed training behavior, as it provided stable convergence without excessive fluctuations in the training loss. A 50% dropout rate and L2 regularization were also applied to both models to strengthen regularization and reduce overfitting. Table 3 summarizes the training settings of LSTM models.

To evaluate the performance of the LSTM predictive models, regression-based error metrics such as Mean Absolute Error (MAE), Mean Squared Error (MSE), Root Mean Squared Error (RMSE), and coefficient of determination (R-Squared) were used to quantify the discrepancy between predicted and actual values. Smaller MAE, MSE, and RMSE values indicate higher forecasting accuracy, whereas an R-Squared value closer to 100% shows a stronger correlation between predicted and actual values.

$$MAE = \frac{1}{N}\sum_{i=1}^{n} |Y_{actual} - Y'_{predicted}| \tag{9}$$

$$MSE = \frac{1}{N}\sum_{i=1}^{n} \left(Y_{actual} - Y'_{predicted}\right)^2 \tag{10}$$

$$RMSE = \sqrt{\frac{1}{N}\sum_{i=1}^{n} \left(Y_{actual} - Y'_{predicted}\right)^2} \tag{11}$$

$$R^2 = 1 - \frac{\sum_{i=1}^{n}\left(Y_{actual} - Y'_{predicted}\right)^2}{\sum_{i=1}^{n}(Y_{actual} - Y_{mean})^2} \tag{12}$$

Table 3. Summary of LSTM training settings

	LSTM Solar PV Energy Generation Prediction	LSTM Load Demand Prediction
Layer	• 1 input (32 neurons) • 1 hidden (50 neurons) • 1 output (1 neuron)	• 1 input (30 neurons) • 1 hidden (50 neurons) • 1 output (1 neuron)
No. of Epochs	2000	2000
Optimizer	Adam	Adam
Learning Rate	0.01	0.01
Type of Learning Rate	Constant	Constant
L2 Regularization	0.01	0.0001

2.5. Problem Formulation

2.5.1. Performance Evaluation Metric

The economic performance of the proposed LSTM-RBC-based EMS is formulated by coordinating the solar PV system, BESS, and the main grid to meet residential load demand. The primary objective is to minimize the total operating cost associated with the power exchange with the main grid, BESS degradation, and the operation and maintenance (O&M) of the solar PV system under the applicable Malaysian ToU electricity tariff and Solar ATAP scheme. Therefore, the total operating cost over the considered simulation period is formulated as the sum of the main grid cost, BESS degradation cost, and solar PV O&M cost, as given in Eq. (13).

$$C_{total} = \sum_{t=0}^{T} C_{grid,t} + C_{bess,t} + C_{pv(O\&M),t} \tag{13}$$

where C_{total}, $C_{grid,t}$, $C_{bess,t}$, and $C_{pv(O\&M),t}$ represent the total operation cost, main grid, BESS, and solar PV O&M, respectively.

The main grid cost, $C_{grid,t}$, is determined based on the energy imported from and exported to the main grid and their corresponding electricity rates during each operating interval Δt, as expressed in Eq. (14). The first term of Eq. (14) represents the cost of electricity imported from the main grid according to the applicable ToU electricity tariff, whereas the second term represents the offset obtained from electricity exported to the main grid under the Solar ATAP scheme.

$$C_{grid,t} = \left(\lambda_{ToU,t} \cdot P_{GIm,t} \cdot \Delta t\right)\mu_{GIm,t} - \left(\lambda_{ATAP,t} \cdot P_{GEx,t} \cdot \Delta t\right)\mu_{GEx,t} \tag{14}$$

where $P_{GIm,t}$ and $P_{GEx,t}$ denote the power imported from and exported to the main grid, respectively, while $\mu_{GIm,t}$ and $\mu_{GEx,t}$ represent the binary variables associated with the grid import and export operating states. The role of these binary variables is further described in Section 2.5.2.

In this study, the applicable ToU electricity tariff, $\lambda_{ToU,t}$, is represented by the combination of the energy, capacity, and network charges, as expressed in (15). The retail charge is excluded from the calculation since it is generally imposed as a fixed monthly charge and does not vary with the hourly electricity consumption. Among the considered tariff components, only the energy charge varies according to the applicable ToU period, with the corresponding rate determined based on whether the operating interval Δt falls within the peak or off-peak period, as summarized in **Table 2**.

$$\lambda_{ToU,t} = \begin{cases} C_{peak} + C_{capacity} + C_{network}, & t \in \tau_{peak} \\ C_{offpeak} + C_{capacity} + C_{network}, & t \in \tau_{offpeak} \end{cases} \tag{15}$$

https://doi.org/10.31436/iiumej.v27i3.4635

where C_{peak} and $C_{offpeak}$ denote the applicable peak and off-peak energy charges, respectively, while $C_{capacity}$ and $C_{network}$ represent the capacity and network charges. The sets τ_{peak} and $\tau_{offpeak}$ represent the operating intervals corresponding to the peak and off-peak periods, respectively.

In contrast to the ToU electricity tariff applied to the grid-imported energy, the Solar ATAP export energy offset rate, $\lambda_{ATAP,t}$, is assumed to remain constant throughout the operating period. Therefore, the same export offset rate applies to electricity exported to the main grid, regardless of whether the interval falls within the peak or off-peak period.

Following the formulation of the main grid cost function, the operating cost associated with the BESS, $C_{bess,t}$, is determined by considering the BESS degradation cost incurred during BESS discharge. As shown in Eq. (16), the BESS degradation cost is calculated as the product of the BESS degradation cost coefficient, $\lambda_{deg,t}$, and the BESS discharge power, $P_{dch,t}$, at the operating interval Δt.

$$C_{bess,t} = \lambda_{deg,t} \cdot P_{dch,t} \cdot \Delta t \tag{16}$$

The BESS degradation cost coefficient, $\lambda_{deg,t}$, represents the equivalent degradation cost incurred per unit of energy discharged from the BESS and is expressed in RM/kWh. In this study, the coefficient is estimated based on the BESS capital cost, expected cycle life, battery capacity, and battery round-trip efficiency, as formulated in Eq. (17).

$$\lambda_{deg,t} = \frac{C_{bess\ capital}}{(N_{cycle})(BESS_{capacity})(DoD)(\eta_{rte})} \tag{17}$$

where $C_{bess\ capital}$ denotes the capital cost of the BESS, N_{cycle} is the battery life cycle, $BESS_{capacity}$ denotes the battery capacity, DoD is the allowable depth of discharge, and η_{rte} represents the battery round-trip efficiency.

In addition to the main grid and BESS costs, the O&M cost of the solar PV system, $C_{pv(O\&M),t}$, is also included in the overall performance evaluation metric to account for the recurring costs required to ensure reliable operation of the solar PV system. As expressed in Eq. (18), the solar PV O&M cost is calculated as the product of the PV O&M cost coefficient, $\lambda_{pv(O\&M),t}$, and the solar PV power output, $P_{pv,t}$, over the operating interval Δt.

$$C_{pv(O\&M),t} = \lambda_{pv(O\&M),t} \cdot P_{pv,t} \cdot \Delta t \tag{18}$$

The PV O&M cost coefficient, $\lambda_{pv(O\&M),t}$, is expressed in RM/kWh and is determined by allocating the annual solar PV O&M cost over its corresponding annual solar PV energy generation, as expressed in Eq. (19).

$$\lambda_{pv(O\&M),t} = \frac{C_{O\&M\ annual}}{E_{pv\ annual}} \tag{19}$$

where $C_{O\&M\ annual}$ represents the annual solar PV O&M cost, while $E_{pv\ annual}$ denotes the corresponding annual solar PV energy generation.

2.5.2. System Constraints

Several system constraints have been considered in the EMS optimization framework to ensure reliable and stable system operation. One primary constraint is the system power balance constraint. The total power consumption must always satisfy the power balance constraint to ensure that the total power generated is sufficient to meet the residential load demand throughout the scheduling horizon, as defined in Eq. (20). The net power contributions of the BESS and main grid are further defined in Eq. (21) and Eq. (22), respectively.

$$P_{load,t} = P_{pv,t} + P_{bess,t} + P_{grid,t} \tag{20}$$

$$P_{bess,t} = P_{dch,t}\mu_{dch,t} - P_{ch,t}\mu_{ch,t} \tag{21}$$

$$P_{grid,t} = P_{GIm,t}\mu_{GIm,t} - P_{GEx,t}\mu_{GEx,t} \tag{22}$$

where $P_{load,t}$ denotes the residential load demand, $P_{bess,t}$ is the net BESS power, $P_{grid,t}$ is the net main grid power, $P_{ch,t}$ is the BESS charging power, while $\mu_{ch,t}$ and $\mu_{dch,t}$ are binary variables representing the BESS charging and discharging operating states, respectively.

Similarly, the power exchange between the microgrid and the main grid is constrained to prevent simultaneous electricity import and export within the same operating interval. The binary variables associated with the grid import and export operating states are introduced as defined in Eq. (23).

$$\mu_{GIm,t} + \mu_{GEx,t} \leq 1,\ where\ \mu_{GIm,t}, \mu_{GEx,t} \in \{0,1\} \tag{23}$$

Another important constraint is related to the charging and discharging operations of the BESS, which must be regulated within the allowable charging and discharging power limits to prevent battery degradation, as expressed in Eq. (24) and Eq. (25). In addition, the charging and discharging operations of the BESS must not occur simultaneously, as stated in Eq. (26).

$$0 \leq P_{ch,t} \leq P_{chMAX} \tag{24}$$

$$0 \leq P_{dch,t} \leq P_{dchMAX} \tag{25}$$

$$\mu_{ch,t} + \mu_{dch,t} \leq 1,\ where\ \mu_{ch,t}, \mu_{dch,t} \in \{0,1\} \tag{26}$$

where P_{chMAX} and P_{dchMAX} denote the maximum allowable BESS charging and discharging power, respectively.

The SoC, which represents the percentage of available energy stored in the BESS relative to its rated capacity, is an important parameter for determining the BESS operational state. The SoC dynamics can be estimated using Eq. (27). The BESS SoC is commonly regulated within predefined minimum and maximum operating limits, as in Eq. (28), to protect the battery and preserve lifetime.

$$SoC_{t+1} = SoC_t + \frac{(P_{ch,t})(\eta_{bess})(\Delta t)}{BESS_{capacity}}\mu_{ch,t} - \frac{(P_{dch,t})(\Delta t)}{(BESS_{capacity})(\eta_{bess})}\mu_{dch,t} \tag{27}$$

$$SoC_{MIN} \leq SoC_t \leq SoC_{MAX} \tag{28}$$

where SoC_{t+1} and SoC_t denote the BESS SoC at the next and current operating intervals, respectively, η_{bess} is the BESS efficiency, while SoC_{MIN} and SoC_{MAX} are the minimum and maximum allowable BESS SoC limits, respectively.

2.5.3. Sizing of Solar PV System

The sizing of the solar PV system is estimated based on the daily load demand, available peak sun hours, and the overall solar PV system efficiency, as shown in Eq. (29).

$$PV_{capacity} = \frac{E_{daily\ load}}{(PSH)(\eta_{system})} \tag{29}$$

where $PV_{capacity}$ is the required rated capacity of the solar PV system in kWp, $E_{daily\ load}$ denotes the total daily load consumption in kWh, PSH represents the average peak sun hours, and η_{system} is the overall efficiency of the solar PV system.

Based on the average hourly solar PV energy generation trend in **Figure 7**, the selected location experiences approximately 5 peak sun hours per day. The overall solar PV system efficiency, η_{system}, is assumed to be 0.7, accounting for various system losses such as temperature effects, wiring, and inverter losses.

Once the required installed PV capacity is obtained, the number of solar PV panels can be determined using Eq. (30).

$$Quantity\ of\ PV\ panels = \frac{PV_{capacity}}{P_{max}} \tag{30}$$

where P_{max} is the peak power of the solar PV panel, based on the specifications provided in **Table 1**.

2.5.4. Sizing of BESS

The sizing of BESS involves the estimation of the required battery capacity capable of storing excess energy generated by RES and supporting the load demand during periods of insufficient generation. Proper BESS sizing is essential to ensure reliable microgrid operation, improve RES utilization, and maintain power-balance stability within the microgrid. In this study, the battery capacity is estimated based on the total daily load consumption, required number of autonomy days, battery depth of discharge, and battery efficiency, as expressed in Eq. (31).

$$BESS_{capacity} = \frac{(E_{daily\ load})(Day_{auto})}{(DoD)(\eta_{bess})} \tag{31}$$

where Day_{auto} denotes the specified number of autonomy days and η_{bess} represents the battery efficiency.

2.6. Control Strategies

2.6.1. Load Following

Figure 10 shows the flowchart of the LF control strategy for the grid-connected microgrid with a solar PV system and BESS. This strategy is categorized into four predefined control rules.

- Rule 1: If $P_{pv,t} > P_{load,t}$, $P_{pv,t}$ supplies the load demand while the excess power is used to charge the BESS. If the BESS reaches full charge, any remaining excess power is exported to the main grid.
- Rule 2: If $P_{pv,t} = P_{load,t}$, $P_{pv,t}$ is fully used to meet the load demand.
- Rule 3: If $P_{pv,t} \leq P_{load,t}$ and $SoC_t \geq SoC_{MIN}$, BESS discharges to serve the net load. In the case of $P_{pv,t} + P_{bess,t} < P_{load,t}$, the main grid will serve the net load.
- Rule 4: If $P_{pv,t} \leq P_{load,t}$ and $SoC_t < SoC_{MIN}$, the main grid will serve the net load.

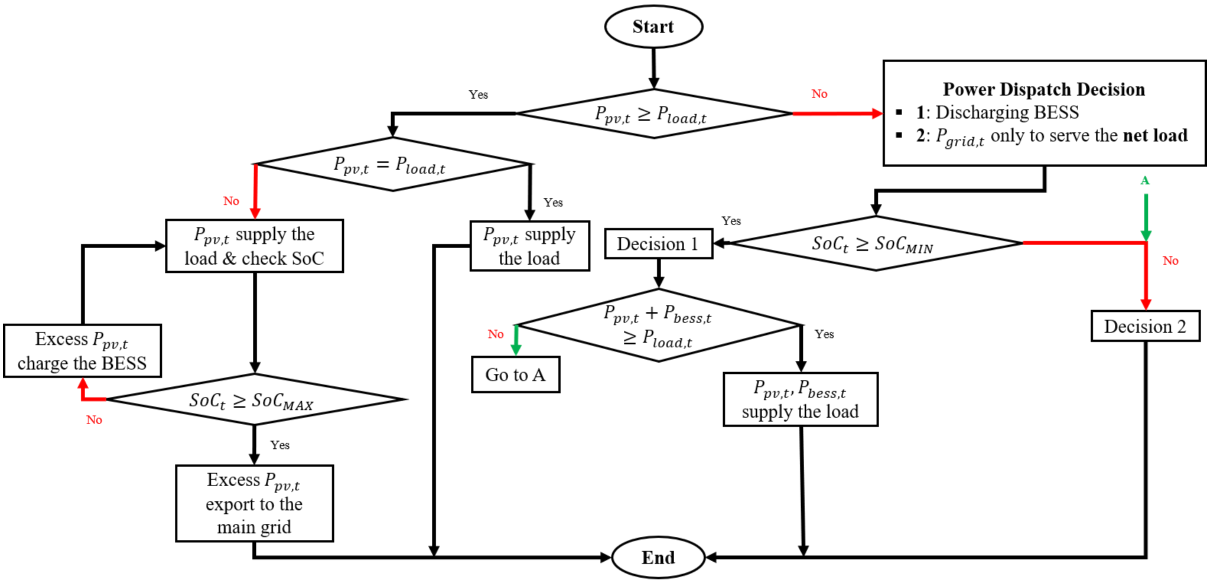

Figure 10. Flowchart of LF control strategy for the solar PV, BESS, and main grid

2.6.2. Cycle Charging

Figure 11 shows the flowchart of the CC control strategy for the same grid-connected microgrid system configuration. This strategy is categorized into four predefined control rules.

- Rule 1: The operating condition is similar to Rule 1 of the LF strategy.
- Rule 2: The operating condition is similar to Rule 2 of the LF strategy.
- Rule 3: If $P_{pv,t} \leq P_{load,t}$ and $SoC_t \geq SoC_{MIN}$, BESS discharges to serve the net load. However, in the case of $P_{pv,t} + P_{bess,t} < P_{load,t}$, the load demand will be fully served by the main grid.
- Rule 4: If $P_{pv,t} \leq P_{load,t}$ and $SoC_t < SoC_{MIN}$, the load demand will be fully served by the main grid. Any excess $P_{pv,t}$ will follow the operating condition in Rule 1, but following flow B.

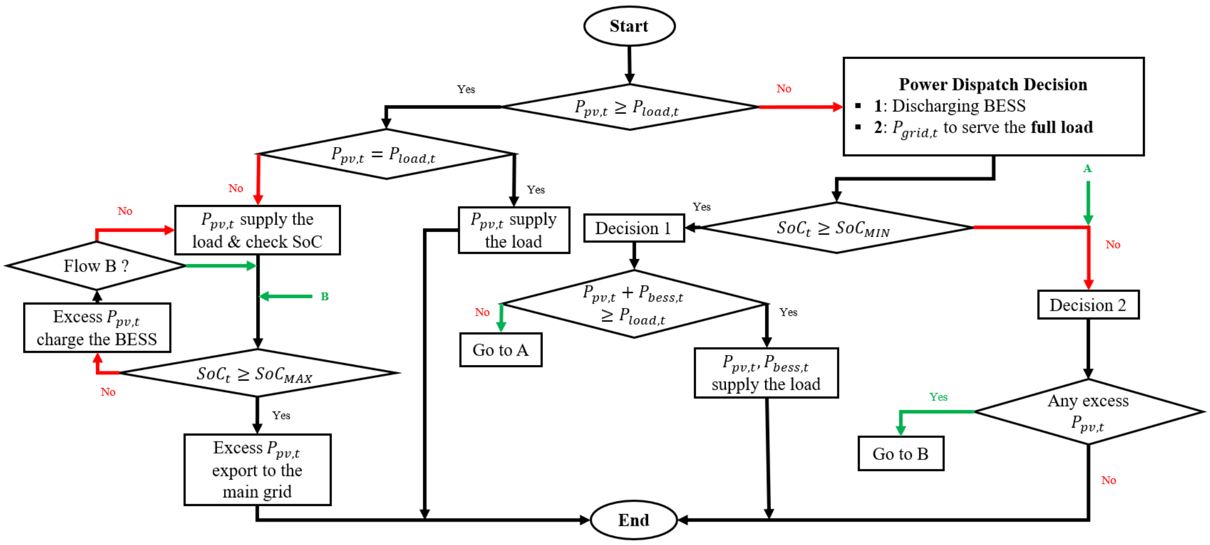

Figure 11. Flowchart of CC control strategy for the solar PV, BESS, and main grid

2.6.3. LSTM-Load Following

Figure 12 shows the flowchart of the LSTM-LF control strategy for the same grid-connected microgrid system configuration. In contrast with the conventional LF control strategy, the proposed LSTM-LF strategy involves forecast information on future solar PV energy generation, $P'_{pv,t}$, and residential load demand, $P'_{load,t}$, together with the corresponding future ToU electricity tariff, $\lambda'_{ToU,t}$, into the control decision-making process. The operation of this strategy is categorized into seven different predefined control rules.

- Rule 1: If $P_{pv,t} > P_{load,t}$, $P'_{pv,t} < P'_{load,t}$ and low $\lambda'_{ToU,t}$, $P_{pv,t}$ supplies the load demand while the BESS charges partially. If the BESS reaches its maximum SoC, it exports any remaining excess power to the main grid.
- Rule 2: If $P_{pv,t} > P_{load,t}$, $P'_{pv,t} < P'_{load,t}$ and high $\lambda'_{ToU,t}$, $P_{pv,t}$ supplies the load demand while the BESS charges aggressively. If the BESS reaches its maximum SoC, it exports any remaining excess power to the main grid.
- Rule 3: If $P_{pv,t} > P_{load,t}$, $P'_{pv,t} > P'_{load,t}$ and low $\lambda'_{ToU,t}$, $P_{pv,t}$ supplies the load demand while the BESS charges moderately. If the BESS reaches its maximum SoC, it exports any remaining excess power to the main grid.
- Rule 4: If $P_{pv,t} > P_{load,t}$, $P'_{pv,t} > P'_{load,t}$ and high $\lambda'_{ToU,t}$, $P_{pv,t}$ supplies the load demand while the BESS charges aggressively. If the BESS reaches its maximum SoC, any remaining excess power is exported to the main grid.
- Rule 5: The operating condition is similar to Rule 2 of the LF strategy.
- Rule 6: The operating condition is similar to Rule 3 of the LF strategy.
- Rule 7: The operating condition is similar to Rule 4 of the LF strategy.

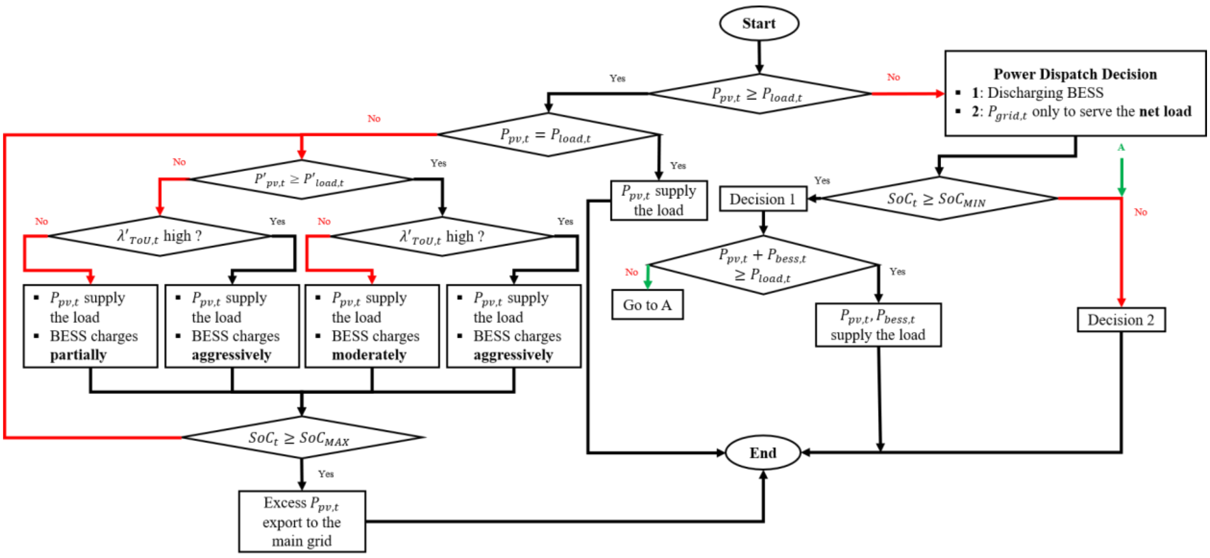

Figure 12. Flowchart of LSTM-LF control strategy for the solar PV, BESS, and main grid

2.6.4. LSTM-Cycle Charging

Figure 13 shows the flowchart of the LSTM-CC control strategy for the same grid-connected microgrid system configuration. Similar to the LSTM-LF strategy, the proposed LSTM-CC strategy involves forecast information on future solar PV energy generation, $P'_{pv,t}$, and residential load demand, $P'_{load,t}$, together with the corresponding future ToU electricity tariff, $\lambda'_{ToU,t}$, into the control decision-making process. This strategy is categorized into seven predefined control rules.

- Rule 1: The operating condition is similar to Rule 1 of the LSTM-LF strategy.
- Rule 2: The operating condition is similar to Rule 2 of the LSTM-LF strategy.
- Rule 3: The operating condition is similar to Rule 3 of the LSTM-LF strategy.
- Rule 4: The operating condition is similar to that in Rule 4 of the LSTM-LF strategy.
- Rule 5: The operating condition is similar to that in Rule 2 of the LF strategy.
- Rule 6: The operating condition is similar to that in Rule 3 of the CC strategy.
- Rule 7: The operating condition is similar to that in Rule 4 of the CC strategy.

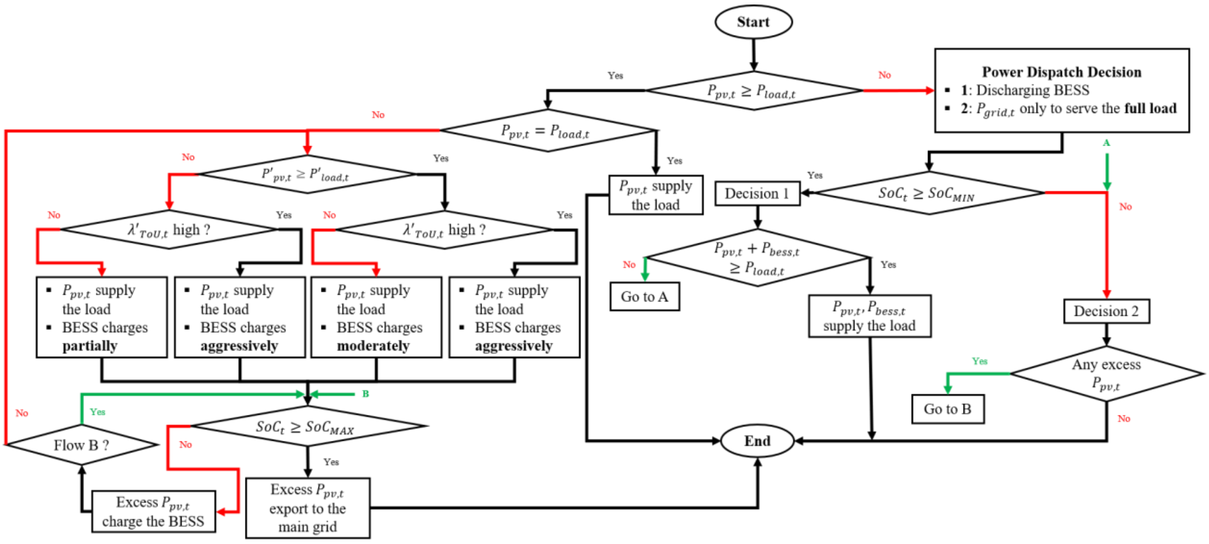

Figure 13. Flowchart of LSTM-CC control strategy for the solar PV, BESS, and main grid

3. RESULTS AND DISCUSSION

3.1. Analysis of LSTM Predictive Models Performance

Table 4 summarizes the performance comparison between the developed LSTM and baseline Feedforward Neural Network (FFNN) predictive models for solar PV energy generation and load demand forecasting using the training, validation, and test datasets. To ensure a fair comparison, the FFNN predictive models were developed using the same input variables, data preprocessing procedures, and training settings as the LSTM predictive models. The only difference is that the FFNN predictive models replace the LSTM layer with a feedforward fully connected layer.

For the solar PV energy generation forecasting, the developed LSTM model achieved MAE values of 0.113933 kWh, 0.079352 kWh, and 0.081602 kWh for the training, validation, and test datasets, respectively. Similarly, the MSE values were 0.045747 kWh^2, 0.019729 kWh^2, and 0.019591 kWh^2, while the RMSE values were 0.213836 kWh, 0.139233 kWh, and 0.139149 kWh. The model also achieved high R-Squared values of 94.93%, 97.83%, and 97.88% for the training, validation, and test datasets, respectively. Compared with the FFNN model, the LSTM consistently achieved lower prediction errors and higher R-Squared values across all datasets, demonstrating its better ability to model and capture the nonlinear relationship between input weather variables and solar PV energy generation. Furthermore, the comparable performance on the validation and test datasets shows that the LSTM model generalizes well to unseen data without significant performance degradation, indicating minimal overfitting.

Figure 14(a) shows the actual and predicted solar PV energy generation profiles for a single solar PV system from 11th to 21st September 2025. In the figure, the red solid line denotes the actual energy generation, while the blue dashed line represents the predicted values. As shown in the figure, the predicted profile closely follows the actual solar PV energy generation pattern, with only minor deviations during the spikes, demonstrating the developed LSTM model's ability to accurately forecast short-term solar PV output.

Similarly, Table 4 shows that the developed LSTM model also outperformed the FFNN model in residential load demand forecasting. The developed LSTM model achieved MAE values of 0.040838 kWh, 0.016715 kWh, and 0.016092 kWh for the training, validation, and test datasets, respectively. The corresponding MSE values were 0.004079 kWh^2, 0.000557 kWh^2, and 0.000521 kWh^2, while the RMSE values were 0.063749 kWh, 0.023357 kWh, and 0.022831 kWh. In addition, the model achieved R-Squared values of 95.24%, 99.21%, and 99.19%, indicating excellent predictive capability across all datasets. Compared with the FFNN model, the LSTM consistently produced lower prediction errors and higher coefficients of determination, indicating that its memory-based architecture is more effective in capturing the sequential patterns in residential load demand data. Furthermore, the comparable validation and test results indicate the robustness and generalization capability of the developed LSTM model for residential load demand prediction.

Table 4. Performance comparison of the developed LSTM and the baseline FFNN

	Performance of LSTM Predictive Models					
	Solar PV Energy Generation			**Load Demand**		
	Training	**Validation**	**Test**	**Training**	**Validation**	**Test**
MAE (kWh)	0.113933	0.079352	0.081602	0.040838	0.016715	0.016092
MSE (kWh^2)	0.045747	0.019729	0.019591	0.004079	0.000557	0.000521
RMSE (kWh)	0.213836	0.139233	0.139149	0.063749	0.023357	0.022831
R-Squared (%)	94.93	97.83	97.88	95.24	99.21	99.19
	Performance of FFNN Predictive Models					
MAE (kWh)	0.146536	0.081079	0.086748	0.046429	0.023673	0.021795
MSE (kWh^2)	0.079981	0.021226	0.022103	0.005286	0.001071	0.000804
RMSE (kWh)	0.282509	0.144911	0.147929	0.072555	0.032290	0.028354
R-Squared (%)	91.16	97.59	97.61	93.53	98.69	98.86

Figure 14(b), (c) and (d) present the predicted load demand profiles of the three selected Malaysian residential load types, namely terrace house, apartment, and condominium, from 11th to 21st September 2025. The red solid line denotes the actual values, whereas the blue dashed line represents the predicted values. Based on these figures, the predicted load demand closely follows the actual load demand pattern, with only minor deviations observed during the spikes.

The comparative results demonstrate that the developed LSTM models consistently outperformed the baseline FFNN models for both solar PV energy generation and residential load demand forecasting. The LSTM achieved lower MAE, MSE, and RMSE values, along with higher R-Squared values, across the training, validation, and test datasets. The LSTM's improved performance can be attributed to its ability to retain and use information from previous time steps, enabling it to capture sequential patterns that are difficult to represent with the conventional feedforward architecture of the FFNN models. In addition, the training and validation loss values remained closely aligned throughout the 2000 training epochs, suggesting stable convergence with minimal overfitting. The comparable validation and test performance further demonstrates the developed LSTM models' generalization capability on unseen data. These findings justify selecting the developed LSTM predictive models for

https://doi.org/10.31436/iiumej.v27i3.4635

integration into the proposed hybrid EMS, where accurate short-term forecasting is essential to support effective energy management and control decisions.

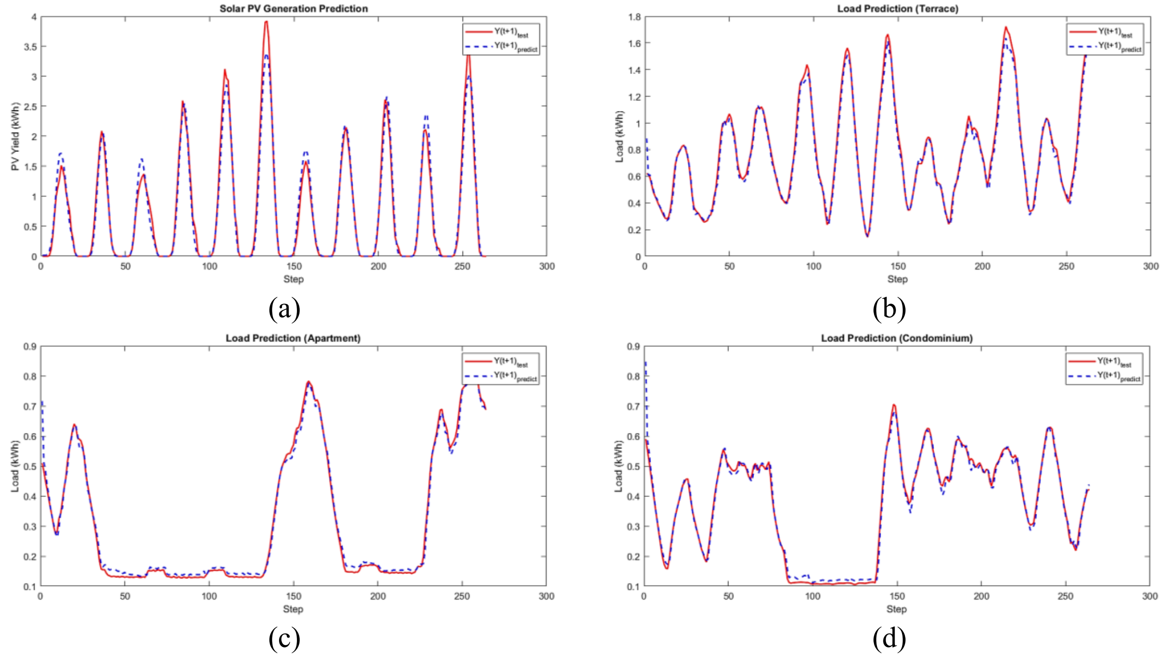

Figure 14. Predicted patterns of (a) solar PV energy generation, (b) load demand for a terrace house, (c) load demand for an apartment house, and (d) load demand for a condominium house, between 11th and 21st September 2025

3.2. Evaluation of the Proposed EMS Performance

Following the successful development of LSTM models for solar PV energy generation and load demand forecasting, this section presents the performance evaluation of the proposed LSTM-RBC-based EMS (LSTM-LF and LSTM-CC). It compares performance with the conventional RBC-based EMS (LF and CC) in managing the operation of the grid-connected residential microgrid under initial BESS SoC scenarios of 80%, 50%, and 30%. The evaluation considers both the operational and economic performance of the EMS, including the power flow analysis, the BESS SoC behavior under ToU electricity pricing, the grid energy exchange, RES utilization, and the associated operating costs, such as grid import and export costs, BESS degradation cost, PV O&M cost, and the overall operating cost of the residential microgrid system.

In this research, all EMS control strategies were evaluated over an 11-day period, from 11th to 21st September 2025, covering 264 operating hours. The evaluation used data for the selected location in Kuala Lumpur, Malaysia (3.1864, 101.7059), as described in the methodology section. **Table 5** summarizes the simulation period, including the day type and the applicable ToU electricity tariff category in Malaysia. The evaluation covers weekdays, weekends, and a holiday (Malaysia Day), allowing the EMS to operate under varying electricity tariff conditions.

The performance evaluation begins with the analysis of the power flow profiles of the four EMS control strategies over the 11-day simulation period, as illustrated in **Figure 15**, **Figure 16**, and **Figure 17**. **Figure 15** compares the power flow profiles under an initial BESS SoC of 80%, while Figures 16 and 17 show the corresponding comparisons for initial BESS SoC scenarios of 50% and 30%. In these figures, the green, blue, red, and purple solid lines represent the power flow profiles of the solar PV system, BESS, main grid, and residential load demand, respectively.

Table 5. Classification of the simulation days according to the day type and the applicable ToU electricity tariff category based on the Malaysian context

Date	Type of Day	Applicable ToU Electricity Tariff
11th September 2025	Weekday	Peak & Off-peak pricing
12th September 2025	Weekday	Peak & Off-peak pricing
13th September 2025	Weekend	Off-peak pricing only
14th September 2025	Weekend	Off-peak pricing only
15th September 2025	Weekday	Peak & Off-peak pricing
16th September 2025	Holiday (Malaysia Day)	Off-peak pricing only
17th September 2025	Weekday	Peak & Off-peak pricing
18th September 2025	Weekday	Peak & Off-peak pricing
19th September 2025	Weekday	Peak & Off-peak pricing
20th September 2025	Weekend	Off-peak pricing only
21st September 2025	Weekend	Off-peak pricing only

As shown in Figure 15(a, c), Figure 16(a, c), and Figure 17(a, c), the conventional RBC-based EMS controls dispatchable DERs solely based on the predefined control rules presented earlier in Figure 10 and Figure 11. The dispatch decisions for the BESS and the main grid were determined only by the instantaneous operating conditions of the residential microgrid, including the net load condition, BESS SoC, and current ToU electricity pricing. As a result, the BESS responded reactively to the variations in solar PV energy generation and residential load demand. In addition, the main grid participated in grid energy exchange only when surplus solar PV energy remained after the BESS reached its maximum allowable SoC, or when the available power from the solar PV system and BESS was insufficient to meet residential load demand.

In contrast, the proposed LSTM-RBC-based EMS retains the predefined RBC structure while incorporating LSTM-based forecasting to anticipate future net load conditions and upcoming ToU electricity tariff periods. Using this predictive information, the EMS can schedule BESS charging and discharging decisions in advance, enabling more economical coordination between the BESS and the main grid. As observed in **Figure 15**(b, d), **Figure 16**(b, d), and **Figure 17**(b, d), this predictive capability results in more active grid energy exchange across all initial BESS SoC scenarios. Unlike the conventional RBC-based EMS, where the main grid serves only as a backup energy source, the proposed hybrid EMS incorporates grid energy exchange into its overall dispatch strategy by importing and exporting electricity based on future net load and the ToU electricity tariff. Although grid energy exchange increases, the proposed hybrid EMS consistently maintains sufficient BESS energy to support residential load demand during high-tariff periods, as shown in **Figure 18**. This coordinated dispatch strategy prioritizes electricity import during lower-tariff periods while minimizing grid import during higher-tariff periods, thereby reducing the overall operating cost of the residential microgrid.

https://doi.org/10.31436/iiumej.v27i3.4635

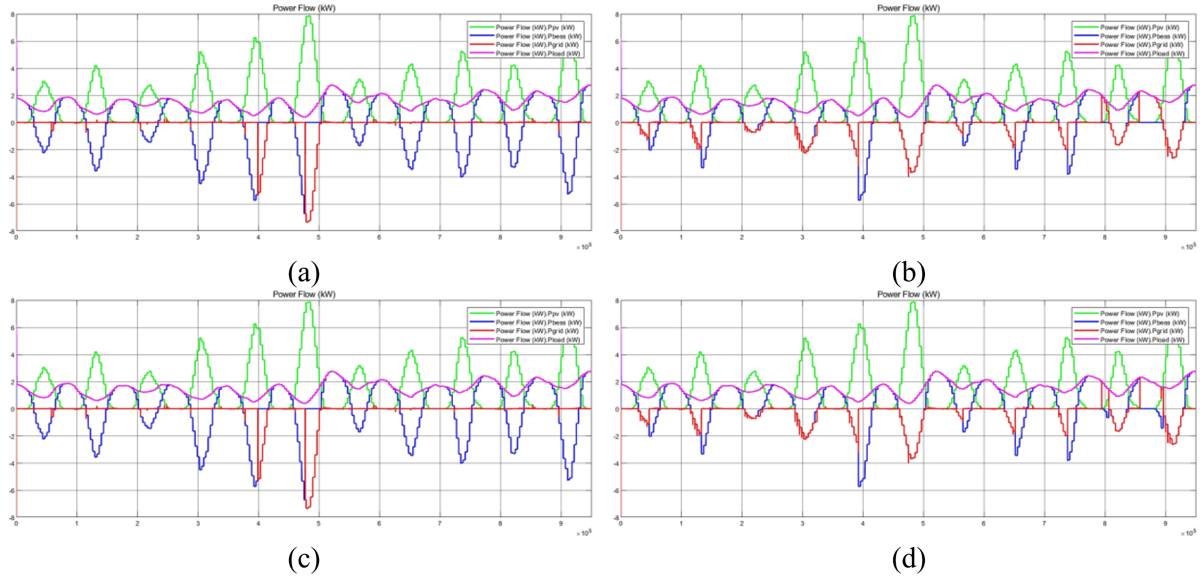

Figure 15. Comparison of power flow profiles for different EMS control strategies at an initial BESS SoC of 80%: (a) LF, (b) LSTM-LF, (c) CC, and (d) LSTM-CC

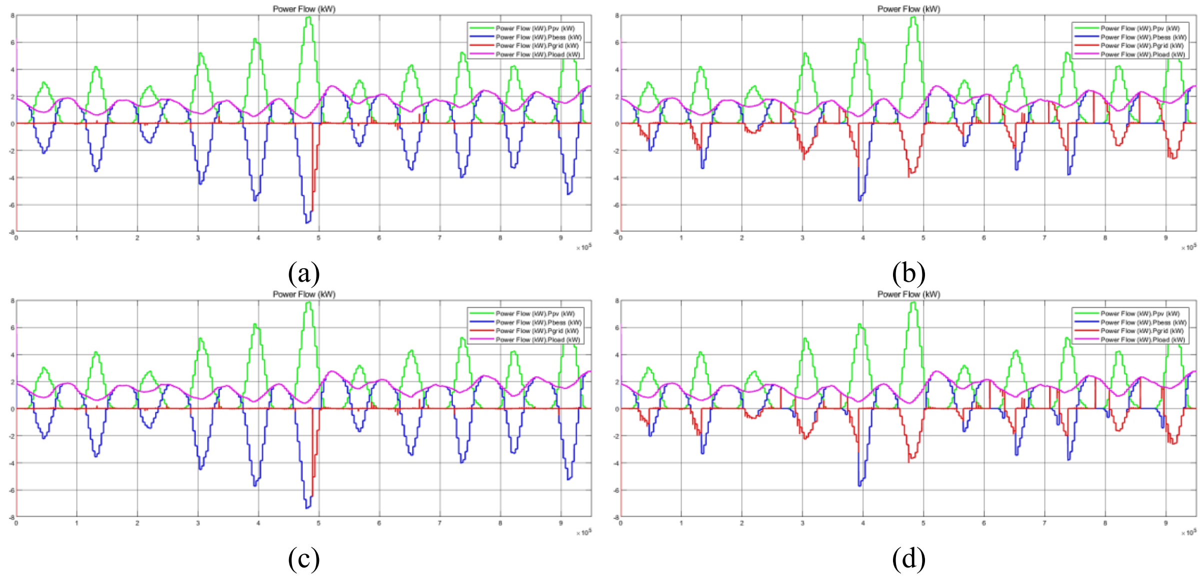

Figure 16. Comparison of power flow profiles for different EMS control strategies at an initial BESS SoC of 50%: (a) LF, (b) LSTM-LF, (c) CC, and (d) LSTM-CC

https://doi.org/10.31436/iiumej.v27i3.4635

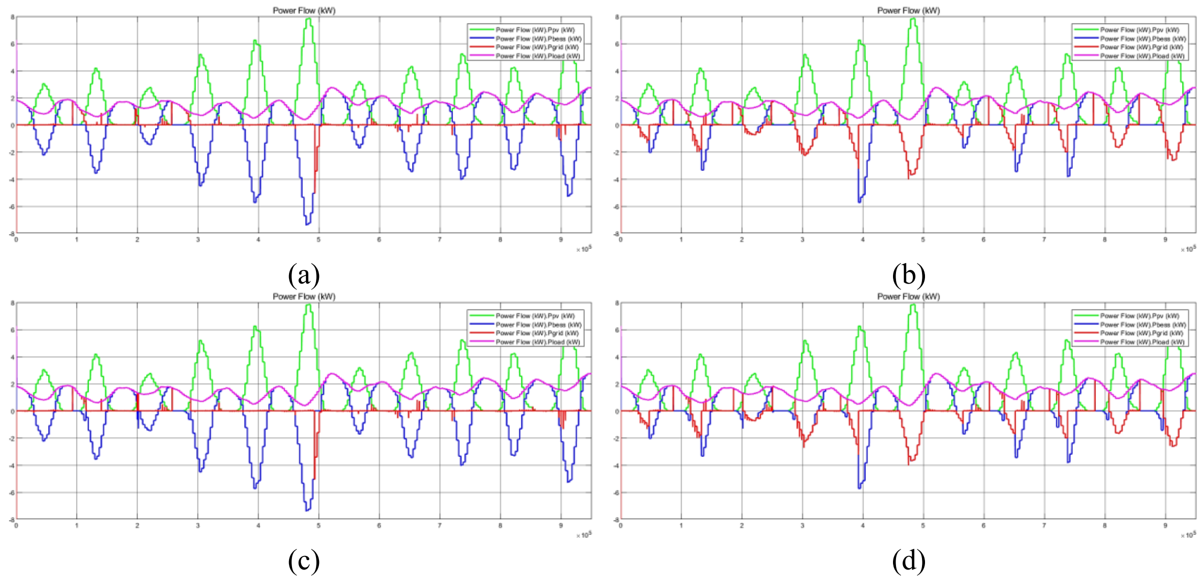

Figure 17. Comparison of power flow profiles for different EMS control strategies at an initial BESS SoC of 30%: (a) LF, (b) LSTM-LF, (c) CC, and (d) LSTM-CC

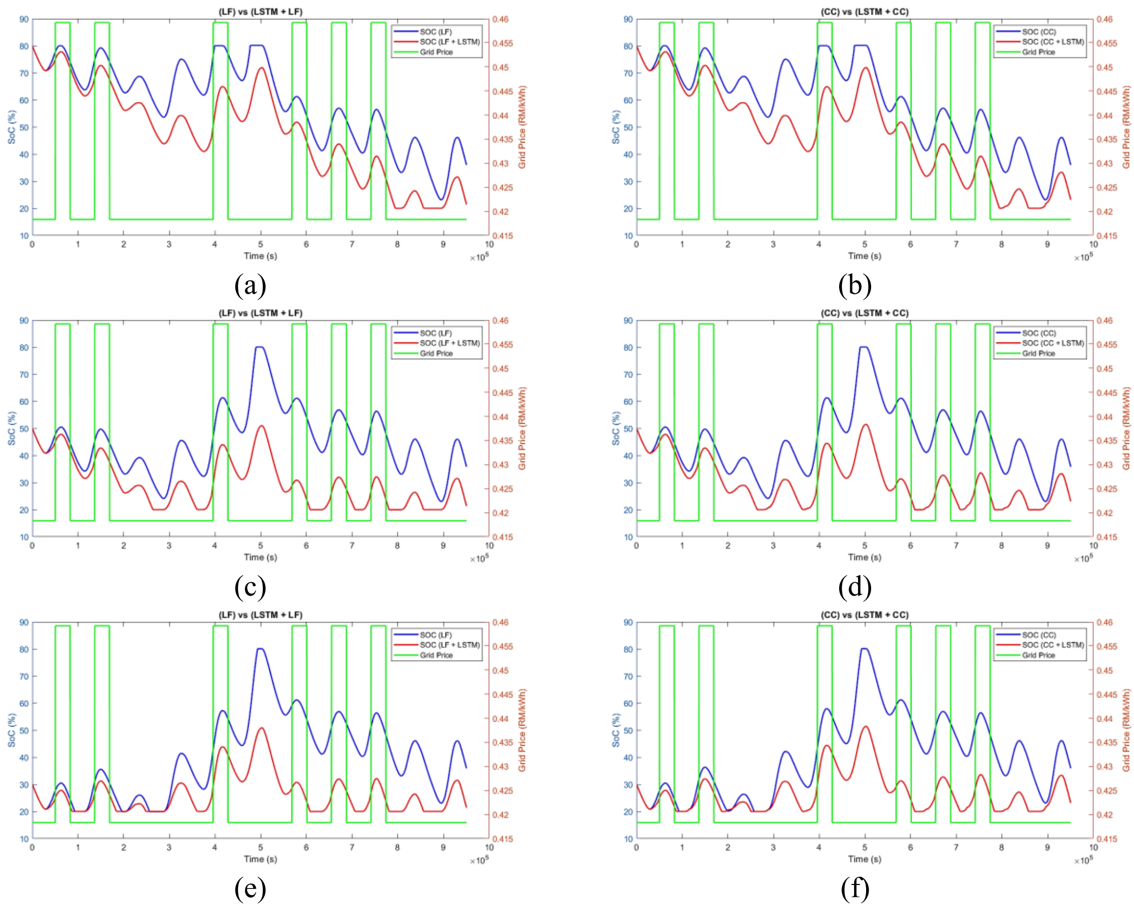

Figure 18. Comparison of BESS SoC profiles under grid ToU electricity prices for the LF and LSTM-LF control strategies at initial SoC of (a) 80%, (c) 50%, and (e) 30%, and for the CC and LSTM-CC control strategies at initial SoC of (b) 80%, (d) 50%, and (f) 30%

Table 6 summarizes the operational and economic performance of the evaluated EMS control strategies under different initial BESS SoC scenarios. The comparison includes key performance indicators such as grid energy import and export, SSR, PV utilization, and associated operating costs, including grid import and export costs, BESS degradation cost, PV O&M cost, and the residential microgrid's total operating cost.

As summarized in **Table 6**, the proposed LSTM-RBC-based EMS consistently achieved a lower total operating cost than the conventional RBC-based EMS across all initial BESS SoC scenarios. This reduction demonstrates the economic benefit of integrating LSTM-based forecasting into the conventional RBC framework, as predicted future net load conditions and upcoming ToU electricity tariff periods enable the EMS to make more informed dispatch decisions rather than relying solely on the microgrid's instantaneous operating conditions. Thus, the BESS and main grid can be coordinated based on both anticipated net load conditions and the corresponding ToU electricity tariff periods.

Table 6. Comparison of the economic and operational performance of different EMS control strategies under varying initial BESS SoC scenarios

		EMS Control Strategy			
		Initial SoC of 80%			
Parameter	**Unit**	**LF**	**CC**	**LSTM-LF**	**LSTM-CC**
Grid Import	kWh	0.06	0.06	24.47	26.82
Grid Export	kWh	48.56	48.56	93.77	93.77
SSR	%	99.98	99.98	93.72	93.12
PV Utilization	%	87.93	87.93	76.70	76.70
Grid Import Cost	RM	0.03	0.03	10.24	11.22
Grid Export Offset	RM	17.97	17.97	34.69	34.69
BESS Degradation Cost	RM	29.33	29.33	26.30	26.40
PV O&M Cost	RM	13.66	13.66	13.66	13.66
Total Operation Cost	RM	25.05	25.05	15.51	16.60
		Initial SoC of 50%			
Grid Import	kWh	0.08	0.08	59.72	62.36
Grid Export	kWh	10.46	10.46	93.81	93.75
SSR	%	99.98	99.98	84.68	84.00
PV Utilization	%	97.40	97.40	76.68	76.70
Grid Import Cost	RM	0.03	0.03	24.98	26.09
Grid Export Offset	RM	3.87	3.87	34.71	34.69
BESS Degradation Cost	RM	29.33	29.33	21.94	22.54
PV O&M Cost	RM	13.66	13.66	13.66	13.66
Total Operation Cost	RM	39.15	39.15	25.88	27.60
		Initial SoC of 30%			
Grid Import	kWh	18.81	19.80	83.43	86.15
Grid Export	kWh	5.18	6.03	93.96	93.85
SSR	%	95.17	94.92	78.59	77.89
PV Utilization	%	98.71	98.50	76.64	76.67
Grid Import Cost	RM	7.87	8.23	34.90	36.04
Grid Export Offset	RM	1.92	2.23	34.77	34.72
BESS Degradation Cost	RM	27.01	27.15	19.00	19.84
PV O&M Cost	RM	13.66	13.66	13.66	13.66
Total Operation Cost	RM	46.63	46.87	32.80	34.81

Compared with the conventional RBC-based EMS, the proposed hybrid EMS showed higher grid energy import and export values. However, this does not mean that the residential microgrid relies heavily on the main grid; it reflects a more strategic use of grid energy exchange. By using future net load and the ToU electricity tariff schedule, the proposed hybrid

EMS prioritizes grid electricity import during lower ToU tariff periods while minimizing grid import during higher tariff periods. Meanwhile, surplus solar PV energy that cannot be used by the residential load or stored in the BESS is exported to the main grid, providing an energy offset under the Solar ATAP scheme. Although the proposed hybrid EMS strategy involves more grid energy exchange, it does not necessarily increase operating costs, as costs depend on both the amount and timing of energy exchanged with the grid.

However, the proposed hybrid EMS introduces trade-offs between microgrid SSR and local RES utilization. As shown in Table 6, the proposed hybrid EMS achieved lower SSR and PV utilization than the conventional RBC-based EMS. The reduction in SSR is mainly due to greater grid imports during lower ToU tariff periods, allowing the BESS to preserve its SoC for later use during higher-tariff periods. Similarly, the reduction in PV utilization mainly results from exporting more surplus PV energy to the main grid rather than using it locally within the microgrid.

The proposed hybrid EMS also resulted in lower BESS degradation costs than the conventional RBC-based EMS across all evaluated initial SoC scenarios. This shows that predictive BESS scheduling enables more effective coordination of charging and discharging operations, reducing unnecessary battery cycling while maintaining reliable support for the residential load.

Overall, Table 6 demonstrates that integrating LSTM-based predictive models into the conventional RBC framework improves the EMS's operational and economic performance, while introducing trade-offs in SSR and PV utilization. The proposed hybrid EMS achieved a significant reduction in total operating cost by approximately 30% to 40% compared with the RBC-based EMS across different initial BESS SoC scenarios. Although the proposed hybrid EMS results in more active grid energy exchange and noticeably lower SSR and PV utilization, this reflects a trade-off between economic performance and energy self-sufficiency. Active grid energy exchange during favorable ToU electricity tariff periods reduces total operating cost. However, this economic benefit also increases the dependency on the main grid and reduces the utilization of locally generated solar PV energy.

4. CONCLUSION

This research proposed a hybrid EMS that integrates ML-based LSTM predictive models with the conventional RBC strategies, such as LF and CC, with a particular focus on the Malaysian residential microgrid scenario. The proposed hybrid EMS was designed to reduce the residential microgrid's total operating cost through more economical DER coordination under the Malaysian ToU electricity tariff and Solar ATAP scheme. The developed grid-connected microgrid consists of a solar PV system, BESS, and three residential load profiles representing terrace, apartment, and condominium households in Kuala Lumpur, Malaysia. Within the proposed framework, the LSTM predictive models provide one-hour-ahead predictions of solar PV energy generation and load demand, while the RBC strategies use these predictions, along with instantaneous operating conditions, to strategically coordinate DER dispatch.

The simulation results demonstrate that the developed LSTM predictive models consistently outperformed the baseline FFNN models in forecasting both solar PV energy generation and residential load demand. For solar PV energy generation, the LSTM model achieved a test MAE of 0.081602 kWh, MSE of 0.019591 kWh^2, RMSE of 0.139149 kWh, and R-Squared of 97.88%. Similarly, the residential load demand model achieved a test MAE of 0.016092 kWh, MSE of 0.000521 kWh^2, RMSE of 0.022831 kWh, and R-Squared of

99.19%. These results demonstrate that the developed LSTM models can accurately capture short-term variations in solar PV energy generation and residential load demand, providing reliable predictive information for the proposed hybrid EMS.

Leveraging these forecasts, the proposed hybrid EMS achieved a significant reduction in total operating cost by around 30% to 40%, along with lower BESS degradation costs, compared with the RBC-only strategies across different initial BESS SoC scenarios. The predictive information enabled the proposed hybrid EMS to schedule BESS charging and discharging in advance and to coordinate the dispatchable DERs more economically. As a result, the system strategically imported electricity during lower ToU tariff periods, while exporting excess solar PV energy to the main grid when conditions were favorable under the Solar ATAP scheme. At the same time, the BESS SoC was maintained at a level sufficient to support the residential load during high-tariff periods. Although the proposed hybrid EMS increased grid energy exchange and reduced SSR and PV utilization, these trade-offs lowered total operating costs.

Despite the encouraging results, several limitations remain. The performance evaluation was conducted over a relatively short simulation period to maintain computational feasibility while still capturing short-term variations in solar PV energy generation and residential load demand. Although Malaysia's tropical climate generally experiences less seasonal variation than regions with four distinct seasons, a longer evaluation period would still provide a more comprehensive analysis of seasonal variations throughout the year. In addition, the proposed hybrid EMS was validated only through MATLAB Simulink simulation and has not yet been evaluated under real operating conditions. The study is also geographically limited to the weather, residential load, and tariff conditions of Kuala Lumpur, Malaysia, which may not generalize to other locations. Furthermore, the comparative analysis was limited to the baseline FFNN model and conventional RBC strategies; therefore, it does not establish superiority over other forecasting models or advanced EMS techniques. Finally, the study also did not include a statistical uncertainty analysis of the forecasting and EMS performance.

Future research may address these limitations by extending the evaluation to longer and more diverse operating periods and analyzing the proposed hybrid EMS across different geographical locations. Its applicability may also be investigated for islanded microgrid operation, particularly in rural and remote areas with limited access to the main grid. In addition, future studies may explore more advanced EMS strategies, such as Reinforcement Learning, Multi-Criteria Decision Making techniques, and other intelligent optimization methods, to improve the DERs dispatch under dynamic operating conditions. Future studies may also include statistical uncertainty and sensitivity analyses to assess the robustness of forecasting and EMS performance under variations in input data, prediction errors, and system parameters. Last but not least, integrating intraday LSTM prediction may further improve the microgrid's operational and economic performance.

ACKNOWLEDGEMENT

This work is supported by the Ministry of Higher Education (MoHE) Malaysia under the Fundamental Research Grant Scheme FRGS (Ref: FRGS/1/2023/TK07/UIAM/02/5 – Project ID: FRGS23-320-0929).

REFERENCES

[1] L. Fusheng, L. Ruisheng, and Z. Fengquan, "Composition and classification of the microgrid," *Microgrid technology and engineering application*, pp. 11–27, 2016.

[2] "Energy Commission - Voltan Nominal." Accessed: Mar. 20, 2026. [Online]. Available: https://www.st.gov.my/en/web/general/details/144

[3] "Energy transition in Malaysia." Accessed: Mar. 19, 2026. [Online]. Available: https://www.energymonitor.ai/data-insights/energy-transition-in-malaysia/?cf-view

[4] T. B. Lopez-Garcia, A. Coronado-Mendoza, and J. A. Domínguez-Navarro, "Artificial neural networks in microgrids: A review," *Eng. Appl. Artif. Intell.*, vol. 95, p. 103894, Oct. 2020, doi: 10.1016/J.ENGAPPAI.2020.103894.

[5] P. A. Cárdenas, M. Martínez, M. G. Molina, and P. E. Mercado, "Development of Control Techniques for AC Microgrids: A Critical Assessment," *Sustainability 2023, Vol. 15, Page 15195*, vol. 15, no. 21, p. 15195, Oct. 2023, doi: 10.3390/SU152115195.

[6] A. Elmouatamid, R. Ouladsine, M. Bakhouya, N. El Kamoun, M. Khaidar, and K. Zine-Dine, "Review of Control and Energy Management Approaches in Micro-Grid Systems," *Energies 2021, Vol. 14, Page 168*, vol. 14, no. 1, p. 168, Dec. 2020, doi: 10.3390/en14010168.

[7] K. Hassan, T. Trireksani, A. Hussain, and H.-M. Kim, "A Rule-Based Modular Energy Management System for AC/DC Hybrid Microgrids," *Sustainability 2025, Vol. 17, Page 867*, vol. 17, no. 3, p. 867, Jan. 2025, doi: 10.3390/SU17030867.

[8] A. S. Aziz, M. F. N. Tajuddin, M. R. Adzman, M. A. M. Ramli, and S. Mekhilef, "Energy Management and Optimization of a PV/Diesel/Battery Hybrid Energy System Using a Combined Dispatch Strategy," *Sustainability 2019, Vol. 11, Page 683*, vol. 11, no. 3, p. 683, Jan. 2019, doi: 10.3390/SU11030683.

[9] S. Chakraborty, G. Modi, and B. Singh, "A Cost Optimized-Reliable-Resilient-Realtime-Rule-Based Energy Management Scheme for a SPV-BES-Based Microgrid for Smart Building Applications," *IEEE Trans. Smart Grid*, vol. 14, no. 4, pp. 2572–2581, Jul. 2023, doi: 10.1109/TSG.2022.3232283.

[10] M. M. Awad, A. Bhattacharjee, and K. N. Hasan, "Design and Energy Management of Solar PV-BESS Integrated Off-Grid Electric Vehicle Charging Station," *2025 12th National Power Electronics Conference (NPEC)*, pp. 1–6, Dec. 2025, doi: 10.1109/NPEC66512.2025.11450150.

[11] K. Nassereddine, M. Turzynski, H. Bielokha, and R. Strzelecki, "Simulation of energy management system using model predictive control in AC/DC microgrid," *Sci. Rep.*, vol. 15, no. 1, pp. 1–12, Dec. 2025, doi: 10.1038/S41598-025-89036-7.

[12] M. Kaheni, J. Fu, and A. V. Papadopoulos, "Rule-Based Predictive Control for Battery Scheduling in Microgrids Under Power Generation and Load Uncertainties," *IEEE Transactions on Automation Science and Engineering*, vol. 22, pp. 9782–9792, 2025, doi: 10.1109/TASE.2024.3512882.

[13] S. Y. Chen and C. H. Chang, "Optimal Power Flows Control for Home Energy Management With Renewable Energy and Energy Storage Systems," *IEEE Transactions on Energy Conversion*, vol. 38, no. 1, pp. 218–229, Mar. 2023, doi: 10.1109/TEC.2022.3198883.

[14] A. Abbasi, H. A. Khalid, H. Rehman, and A. U. Khan, "A Novel Dynamic Load Scheduling and Peak Shaving Control Scheme in Community Home Energy Management System Based Microgrids," *IEEE Access*, vol. 11, pp. 32508–32522, 2023, doi: 10.1109/ACCESS.2023.3255542.

[15] M. M. Shibl, L. S. Ismail, and A. M. Massoud, "An Intelligent Two-Stage Energy Dispatch Management System for Hybrid Power Plants: Impact of Machine Learning Deployment," *IEEE Access*, vol. 11, pp. 13091–13102, 2023, doi: 10.1109/ACCESS.2023.3243097.

[16] E. Giglio, G. Luzzani, V. Terranova, G. Trivigno, A. Niccolai, and F. Grimaccia, "An Efficient Artificial Intelligence Energy Management System for Urban Building Integrating

https://doi.org/10.31436/iiumej.v27i3.4635

Photovoltaic and Storage," *IEEE Access*, vol. 11, pp. 18673–18688, 2023, doi: 10.1109/ACCESS.2023.3247636.

[17] O. Akbulut, M. Cavus, M. Cengiz, A. Allahham, D. Giaouris, and M. Forshaw, "Hybrid Intelligent Control System for Adaptive Microgrid Optimization: Integration of Rule-Based Control and Deep Learning Techniques," *Energies 2024, Vol. 17, Page 2260*, vol. 17, no. 10, p. 2260, May 2024, doi: 10.3390/EN17102260.

[18] "Fahami Tarif Elektrik Anda | TNB Malaysia." Accessed: Aug. 13, 2025. [Online]. Available: https://www.mytnb.com.my/tariff/index.html?v=1.1.34

[19] "Solar ATAP Malaysia 2026 | Cut TNB Bills 90% | No Quota, Apply Anytime." Accessed: Aug. 12, 2026. [Online]. Available: https://solaratap.my/

[20] R. R. Onteru, V. Sandeep, Rupesh, and R. Onteru, "An intelligent model for efficient load forecasting and sustainable energy management in sustainable microgrids," *Discover Sustainability 2024 5:1*, vol. 5, no. 1, pp. 170-, Jul. 2024, doi: 10.1007/s43621-024-00356-6.